

Complete next-to-leading order perturbative QCD prediction for the pion form factor

B. Melić, B. Nizić, and K. Passek*

*Theoretical Physics Division, Rudjer Bošković Institute,
P.O. Box 1016, HR-10001 Zagreb, Croatia*

(January 31, 1998)

We present the results of a complete leading-twist next-to-leading order QCD analysis of the spacelike pion electromagnetic form factor at large momentum transfer Q^2 . We have studied their dependence on the form of the pion distribution amplitude and, out of the four distribution amplitudes considered, found that the final choice should be made between the asymptotic and the Chernyak - Zhitnitsky (CZ) distribution amplitudes. We have also examined the sensitivity of the predictions based on these two distributions to the choice of the renormalization and factorization scales. Choosing the renormalization scale to be of the order of the average virtuality of the particles in the corresponding parton subprocess, we have found that the next-to-leading order prediction for the pion form factor can reliably be calculated at momentum transfers of about 15 GeV^2 and 30 GeV^2 for the asymptotic and the CZ distribution amplitudes, respectively, with the correction to the leading-order results being of the order of $\sim 20\%$. The difference between the results for the asymptotic and the CZ distribution amplitudes is sufficiently large for an unambiguous discrimination between these two distributions when the experimental data are obtained at higher Q^2 values.

13.40.Gp, 12.38.Bx

I. INTRODUCTION

Exclusive processes involving large-momentum transfer are among the most interesting and challenging tests of quantum chromodynamics (QCD).

The framework for analyzing such processes within the context of perturbative QCD (PQCD) has been developed by Brodsky and Lepage [1], Efremov and Radyushkin [2], and Duncan and Mueller [3] (see Ref. [4] for reviews). They have demonstrated, to all orders in perturbation theory, that exclusive amplitudes involving large-momentum transfer factorize into a convolution of a process-independent and perturbatively incalculable distribution amplitude, one for each hadron involved in the amplitude, with a process-dependent and perturbatively calculable hard-scattering amplitude.

Within the framework developed in Refs. [1,2,3], leading-order (LO) predictions have been obtained for many exclusive processes. It is well known, however, that, unlike in QED, the LO predictions in PQCD do not have much predictive power, and that higher-order corrections are essential for many reasons. In general, they have a stabilizing effect reducing the dependence of the predictions on the schemes and scales. Therefore, to achieve a complete confrontation between theoretical predictions and experimental data, it is very important to know the size of the radiative corrections to the LO predictions. The list of exclusive processes at large-momentum transfer analyzed at next-to-leading order (NLO) is very short and includes only three processes: the pion electromagnetic form factor [5,6,7,8,9,10], the pion transition form factor [10,11,12], and photon-photon annihilation into two flavor-nonsinglet helicity-zero mesons, $\gamma\gamma \rightarrow M\bar{M}$ ($M = \pi, K$) [13].

In leading twist, the pion electromagnetic form factor (the simplest exclusive quantity) can be written as

$$F_\pi(Q^2) = \int_0^1 dx \int_0^1 dy \Phi^*(y, \mu_F^2) T_H(x, y, Q^2, \mu_R^2, \mu_F^2) \Phi(x, \mu_F^2). \quad (1.1)$$

Here $\Phi(x, \mu_F^2)$ is the pion distribution amplitude, i.e., the probability amplitude for finding the valence $q_1\bar{q}_2$ Fock state in the initial pion with the constituents carrying the longitudinal momentum xP and $(1-x)P$; $T_H(x, y, Q^2, \mu_R^2, \mu_F^2)$ is the hard-scattering amplitude, i.e., the amplitude for a parallel $q_1\bar{q}_2$ pair of the total momentum P hit by a virtual photon γ^* of momentum q to end up as a parallel $q_1\bar{q}_2$ pair of momentum $P' = P + q$;

*Electronic addresses: melic@thphys.irb.hr, nizic@thphys.irb.hr, passek@thphys.irb.hr

$\Phi^*(y, \mu_F^2)$ is the amplitude for the final state $q_1 \bar{q}_2$ to fuse back into a pion; $Q^2 = -q^2$ is the momentum transfer in the process and is supposed to be large; μ_R is the renormalization (or coupling constant) scale and μ_F is the factorization (or separation) scale at which soft and hard physics factorize.

The hard-scattering amplitude T_H can be calculated in perturbation theory and represented as a series in the QCD running coupling constant $\alpha_S(\mu_R^2)$. The function Φ is intrinsically nonperturbative, but its evolution can be calculated perturbatively.

Although, the PQCD approach of Refs. [1,2,3] undoubtedly represents an adequate and efficient tool for analyzing exclusive processes at very large momentum transfer, its applicability to these processes at experimentally accessible momentum transfer has long been debated and attracted much attention. The concern has been raised [14,15] that, even at very large momentum transfer, important contributions to these processes could arise from nonfactorizing end-point contributions of the distribution amplitudes with $x \sim 1$. It has been shown, however, that the incorporation of the Sudakov suppression effectively eliminates these soft contributions and that the PQCD approach to the pion form factor begins to be self-consistent for a momentum transfer of about $Q > 4 \text{ GeV}^2$ [16] (see also Ref. [17]).

To obtain the complete NLO prediction for the pion form factor requires calculating NLO corrections to both the hard-scattering amplitude and the evolution kernel for the pion distribution amplitude.

The NLO predictions for the pion form factor obtained in Refs. [5,6,7,8,9] are incomplete in so far as only the NLO correction to the hard-scattering amplitude has been considered, whereas the corresponding NLO corrections to the evolution of the pion distribution amplitude have been ignored. Apart from not being complete, the results of the calculations presented in Refs. [5,6,7,8,9] do not agree with one another. It is pointed out in Ref. [9] that this is due to the fact that the hard-scattering amplitudes calculated in [5,6] contain calculational as well as some conceptual errors.

Evolution of the distribution amplitude can be obtained by solving the differential-integral evolution equation, using the moment method. In order to determine the NLO corrections to the evolution of the distribution amplitude, it is necessary to calculate two-loop corrections to the evolution kernel. These have been computed by different authors and the obtained results are in agreement [18]. Because of the complicated structure of these corrections, it was possible to obtain numerically only the first few moments of the evolution kernel [19]. Using these incomplete results, the first attempt to include the NLO corrections to the evolution of the distribution amplitude in the NLO analysis of the pion form factor was obtained in Ref. [10]. It was found that the NLO corrections to the evolution of the pion distribution amplitude as well as to the pion form factor were tiny.

Considerable progress has recently been made in understanding the NLO evolution of the pion distribution amplitude [20]. Using conformal constraints, the complete formal solution of the NLO evolution equation has been obtained. Based on this result, it has been found that, contrary to the estimates given in Ref. [10], the NLO corrections to the evolution of the distribution amplitude are rather large. It has been concluded that because of the size of the discovered corrections, and their dependence upon the input distribution amplitude, the evolution of the distribution amplitude has to be included in the NLO analysis of exclusive processes at large momentum transfer.

The purpose of this paper is to present a complete leading-twist NLO QCD analysis of the spacelike pion electromagnetic form factor at large momentum transfer.

The plan of the paper is as follows. To check and verify the results obtained in Ref. [5,6,7,8,9], in Sec. II we carefully calculate all one-loop diagrams contributing to the NLO hard-scattering amplitude for the pion form factor. Our results are in complete agreement with those obtained in Ref. [9]. Making use of the method introduced in Ref. [20], in Sec. III we determine NLO evolutionary corrections to four available candidate pion distribution amplitudes. In Sec. IV several possible choices of the renormalization scale μ_R and the factorization scale μ_F are discussed. In Sec. V we obtain complete NLO predictions for the pion form factor using the four candidate pion distribution amplitudes and different choices of the renormalization and factorization scales, μ_R and μ_F , respectively. We also examine how the assumption of the frozen coupling at low momentum transfer affects our predictions. Section VI is devoted to discussions and some concluding remarks.

II. NLO CORRECTION TO THE HARD-SCATTERING AMPLITUDE

In this section we recalculate the NLO correction to the hard-scattering amplitude for the pion form factor. In leading twist, it is obtained by evaluating the $(q_1 \bar{q}_2) + \gamma^* \rightarrow (q_1 \bar{q}_2)$ amplitude, which is described by the Feynman diagrams in Fig. 1, with massless valence quarks collinear with outgoing mesons. In this evaluation, terms of order m^2/Q^2 are not included and, since the constituents are constrained to be collinear, terms of order k_\perp^2/Q^2 (k_\perp is the average transverse momentum in the meson) are also not taken into account. By definition, T_H is free of collinear singularities and has a well-defined expansion in $\alpha_S(\mu_R^2)$ of the form

$$T_H(x, y, Q^2, \mu_R^2, \mu_F^2) = \alpha_S(\mu_R^2) T_H^{(0)}(x, y, Q^2)$$

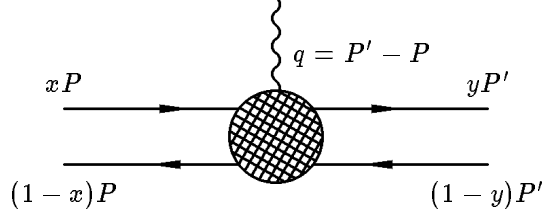


FIG. 1. Feynman diagrams describing the $(q_1 \bar{q}_2) + \gamma^* \rightarrow (q_1 \bar{q}_2)$ amplitude in terms of which the hard-scattering amplitude for the pion form factor is obtained.

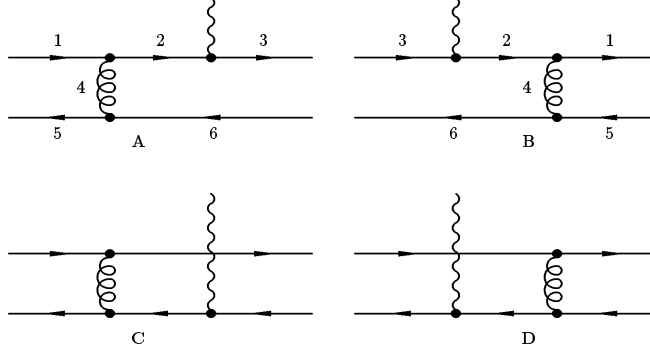


FIG. 2. Lowest-order Feynman diagrams contributing to the $(q_1 \bar{q}_2) + \gamma^* \rightarrow (q_1 \bar{q}_2)$ amplitude.

$$\times \left[1 + \frac{\alpha_S(\mu_R^2)}{\pi} T_H^{(1)}(x, y, \mu_R^2/Q^2, \mu_F^2/Q^2) + \dots \right], \quad (2.1)$$

where

$$\alpha_S(\mu_R^2) = \frac{4\pi}{\beta_0 \ln(\mu_R^2/\Lambda_{QCD}^2)}, \quad (2.2)$$

and

$$\beta_0 = 11 - \frac{2}{3}n_f, \quad (2.3)$$

with n_f being the effective number of quark flavors and Λ_{QCD} is the fundamental QCD parameter.

In the LO approximation (Born approximation) there are only four Feynman diagrams contributing to the $(q_1 \bar{q}_2) + \gamma^* \rightarrow (q_1 \bar{q}_2)$ transition amplitude. They are shown in Fig. 2. Evaluating these diagrams, one finds that the LO hard-scattering amplitude is given by

$$T_H^{(0)}(x, y, Q^2) = \frac{4}{3} \frac{16\pi}{Q^2(1-x)(1-y)}. \quad (2.4)$$

At NLO there are altogether 62 one-loop Feynman diagrams contributing to the hard-scattering amplitude. All these diagrams can be generated from the LO diagrams in Fig. 2 by inserting an internal gluon line. We use the notation where Aij is the diagram obtained from diagram A by inserting the gluon line connecting the lines i and j , where $i, j = 1, 2, \dots, 6$. The number of distinct diagrams that need to be evaluated is 17. They are shown in Fig. 3 with the exception of A33, A55, and A66, which give obviously the same contribution as A11. These diagrams contain ultraviolet (UV) singularities and, owing to the fact that initial- and final-state quarks are massless and onshell, they also contain both infrared (IR) and collinear singularities. We use dimensional regularization in $D = 4 - 2\epsilon$ dimensions to regularize all three types of singularities, distinguishing the poles $1/\epsilon$ by the subscripts UV and IR ($D = 4 - 2\epsilon_{UV} = 4 + 2\epsilon_{IR}$). Soft singularity is always accompanied by two collinear singularities and, consequently, when dimensionally regularized, leads to the double pole $1/\epsilon_{IR}^2$.

The NLO amplitude for the $(q_1 \bar{q}_2) + \gamma^* \rightarrow (q_1 \bar{q}_2)$ quark subprocess can be written as

$$\Delta(x, y, \mu_R^2/Q^2, \mu_F^2/Q^2) = \alpha_S \Delta^{(0)}(x, y, Q^2) \left[1 + \left(\frac{\alpha_S}{\pi} \right) \Delta^{(1)}(x, y, \mu_R^2/Q^2, \mu_F^2/Q^2) \right], \quad (2.5)$$

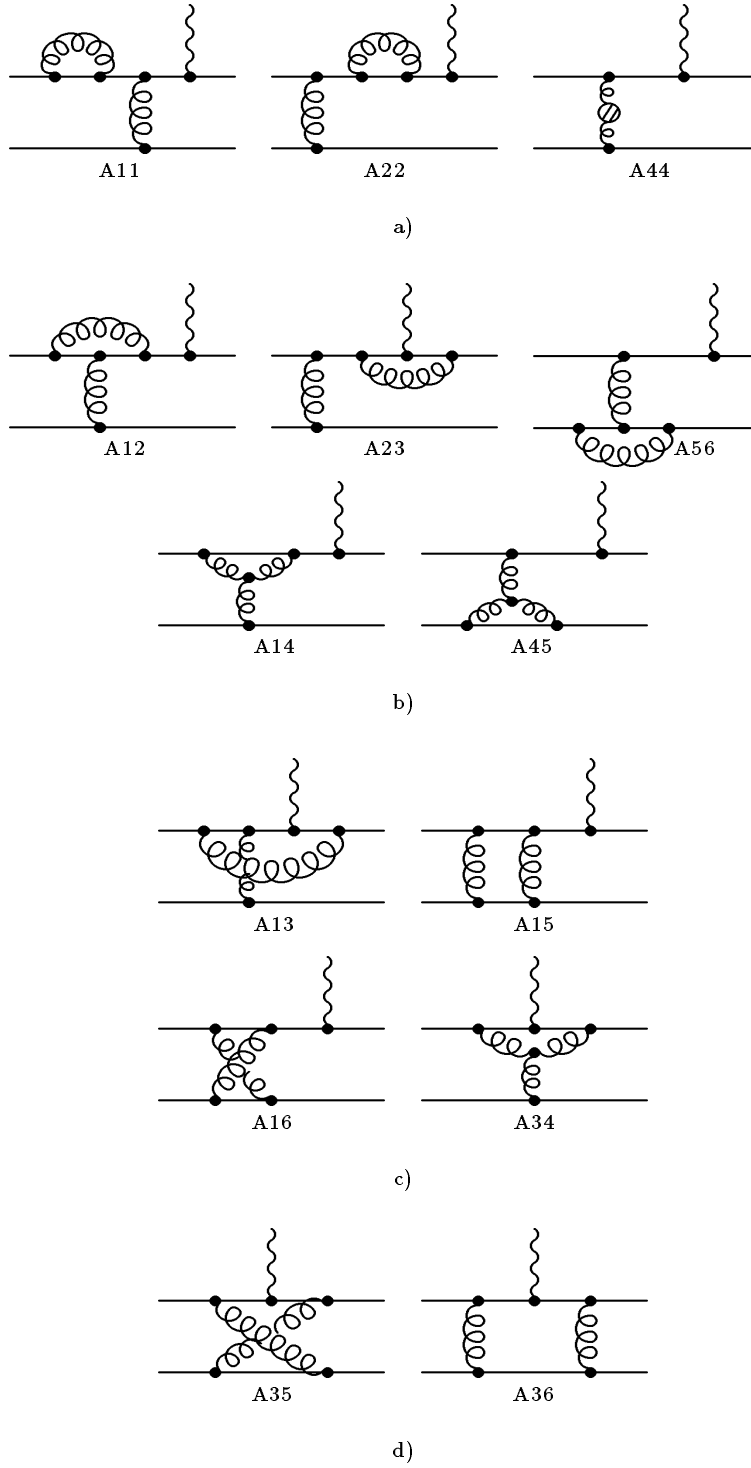


FIG. 3. Distinct one-loop Feynman diagrams contributing to the $(q_1 \bar{q}_2) + \gamma^* \rightarrow (q_1 \bar{q}_2)$ amplitude. The total number of diagrams is 62.

where, obviously,

$$\Delta^{(0)}(x, y, Q^2) = T_H^{(0)}(x, y, Q^2). \quad (2.6)$$

Using the Feynman gauge for the gluon propagator, we have obtained the contributions of the individual diagrams to $\Delta^{(1)}(x, y, \mu_R^2/Q^2, \mu_F^2/Q^2)$, as given in Table I. We have used the following notation:

$$\begin{aligned} \bar{x} &= 1 - x, \quad \bar{y} = 1 - y, \\ \eta_{UV} &= \frac{1}{\epsilon_{UV}} - \gamma - \ln \frac{Q^2}{4\pi\mu_R^2} = \frac{1}{\hat{\epsilon}_{UV}} + \ln \frac{\mu_R^2}{Q^2}, \\ \eta_{IR} &= \frac{1}{\epsilon_{IR}} + \gamma + \ln \frac{Q^2}{4\pi\mu_F^2} = \frac{1}{\hat{\epsilon}_{IR}} - \ln \frac{\mu_F^2}{Q^2}, \\ \tilde{\eta}_{IR} &= \frac{1}{\epsilon_{IR}^2} + \frac{1}{\epsilon_{IR}} \left(\gamma + \ln \frac{Q^2}{4\pi\mu_F^2} \right) + \frac{1}{2} \left(\gamma^2 - \frac{\pi^2}{6} \right) \\ &\quad + \gamma \ln \frac{Q^2}{4\pi\mu_F^2} + \frac{1}{2} \ln^2 \frac{Q^2}{4\pi\mu_F^2}, \\ \frac{1}{\hat{\epsilon}_{UV}} &= \frac{1}{\epsilon_{UV}} - \gamma + \ln(4\pi), \\ \frac{1}{\hat{\epsilon}_{IR}} &= \frac{1}{\epsilon_{IR}} + \gamma - \ln(4\pi). \end{aligned} \quad (2.7)$$

The function $H(x, y)$ appearing in Table I is given by the expression

$$\begin{aligned} H(x, y) &= \frac{1}{1-x-y} \left[\text{Li}_2 \left(\frac{\bar{y}}{x} \right) + \text{Li}_2 \left(\frac{\bar{x}}{y} \right) + \text{Li}_2 \left(\frac{xy}{\bar{x}\bar{y}} \right) \right. \\ &\quad \left. - \text{Li}_2 \left(\frac{x}{\bar{y}} \right) - \text{Li}_2 \left(\frac{y}{\bar{x}} \right) - \text{Li}_2 \left(\frac{\bar{x}\bar{y}}{xy} \right) \right], \end{aligned} \quad (2.8)$$

where $\text{Li}_2(x)$ is the Spence function defined as

$$\text{Li}_2(x) = - \int_0^x \frac{\ln(1-t)}{t} dt. \quad (2.9)$$

The contribution of the one-loop diagram Bij ($i, j = 1, 2, \dots, 6$), generated from the LO diagram B in Fig. 2, is related to the contribution of the corresponding diagram Aij by interchanging x and y . Adding up the contributions of all diagrams, we find

$$\begin{aligned} \Delta^{(1)}(x, y, \mu_R^2/Q^2, \mu_F^2/Q^2) &= C_{UV}(x, y) \frac{1}{\hat{\epsilon}_{UV}} + C_{IR}(x, y) \frac{1}{\hat{\epsilon}_{IR}} \\ &\quad + f_{UV}(x, y, \mu_R^2/Q^2) + f_{IR}(x, y, \mu_F^2/Q^2) + f_C(x, y), \end{aligned} \quad (2.10)$$

where

$$C_{UV}(x, y) = \frac{1}{4} \beta_0, \quad (2.11a)$$

$$C_{IR}(x, y) = \frac{2}{3} [3 + \ln(\bar{x}\bar{y})], \quad (2.11b)$$

and

$$f_{UV}(x, y, \mu_R^2/Q^2) = C_{UV}(x, y) \left[\frac{2}{3} - \ln(\bar{x}\bar{y}) + \ln \frac{\mu_R^2}{Q^2} \right], \quad (2.12a)$$

$$f_{IR}(x, y, \mu_F^2/Q^2) = C_{IR}(x, y) \left[\frac{1}{2} \ln(\bar{x}\bar{y}) - \ln \frac{\mu_F^2}{Q^2} \right], \quad (2.12b)$$

$$\begin{aligned} f_C(x, y) &= \frac{1}{12} [-10 + 20 \ln(\bar{x}\bar{y}) + \ln x \ln y \\ &\quad + \ln \bar{x} \ln \bar{y} - \ln x \ln \bar{y} - \ln \bar{x} \ln y \\ &\quad + (1-x-y)H(x, y) + R(x, y)]. \end{aligned} \quad (2.12c)$$

TABLE I. Contributions to $\Delta^{(1)}(x, y, \mu_R^2/Q^2, \mu_F^2/Q^2)$, defined in (2.5), of Feynman diagrams shown in Fig. 3.

A11	$-\frac{1}{12}(\eta_{UV} + \eta_{IR})$
A22	$-\frac{1}{6}(\eta_{UV} - \ln \bar{y})$
A44	$\frac{1}{8} \left[\left(5 - \frac{2}{3}n_f \right) (\eta_{UV} - \ln(\bar{x}\bar{y})) + \frac{16}{3} - \frac{4}{9}n_f \right]$
A23	$\frac{1}{6} \left(\eta_{UV} + \frac{1+\bar{y}}{y} \ln \bar{y} \right)$
A12	$-\frac{1}{48} \left[\eta_{UV} + 2\eta_{IR} \left(1 + \frac{\bar{x}}{x} \ln \bar{x} \right) - 3 - \frac{\bar{x}}{x} \ln \bar{x} + \ln \bar{y} + \frac{\bar{x}}{x} \ln^2 \bar{x} + 2\frac{\bar{x}}{x} \ln \bar{x} \ln \bar{y} \right]$
A56	$-\frac{1}{48} [\eta_{UV} + 2\eta_{IR}(1 - \ln(\bar{x}\bar{y})) - 2\tilde{\eta}_{IR} - 5 + \ln(\bar{x}\bar{y}) - \ln^2 \bar{x} - \ln^2 \bar{y} - 2\ln \bar{x} \ln \bar{y}]$
A14	$\frac{3}{16} \left[3\eta_{UV} + 2\eta_{IR} \left(1 + \frac{\ln \bar{x}}{x} \right) + 1 + \ln \frac{\bar{x}}{\bar{y}} + \frac{\ln^2 \bar{x}}{x} + 2\frac{\ln \bar{x} \ln \bar{y}}{x} \right]$
A45	$\frac{3}{16} [3\eta_{UV} + 4\eta_{IR} - 1 + \ln(\bar{x}\bar{y})]$
A15	$-\frac{1}{3} \frac{\bar{x}}{x} \left[\eta_{IR} \ln \bar{x} + \ln \bar{x} + \frac{1}{2} \ln^2 \bar{x} + \ln \bar{x} \ln \bar{y} \right]$
A16	$-\frac{1}{24} \left[\tilde{\eta}_{IR} + \eta_{IR} \left(1 + \frac{\ln \bar{x}}{x} + 2\ln x + \ln \bar{y} \right) + \frac{\ln \bar{x}}{x} + 2\ln x + \ln \bar{y} + \frac{1}{2} \frac{\ln^2 \bar{x}}{x} + \ln^2 x \right. \\ \left. + \frac{1}{2} \ln^2 \bar{y} + \frac{\ln \bar{x} \ln \bar{y}}{x} + 2\ln x \ln \bar{y} \right]$
A34	$\frac{3}{8} \left[\eta_{IR} \left(2 + \frac{\ln \bar{x}}{x} + \frac{\ln \bar{y}}{y} \right) - 2 + \ln \bar{x} + \ln \bar{y} + \frac{\bar{x} + \bar{y}}{xy} \ln \bar{x} \ln \bar{y} + \frac{1}{2x} \ln^2 \bar{x} + \frac{1}{2y} \ln^2 \bar{y} \right]$
A13	$\frac{1}{24} \left\{ \tilde{\eta}_{IR} + \eta_{IR} \left(\frac{\bar{x}}{x} \ln \bar{x} + \ln x + \ln y \right) + 1 \right. \\ \left. + \frac{\bar{x}}{2x} \ln^2 \bar{x} + \frac{1}{2} \ln^2 x + \frac{1}{2} \ln^2 y + \ln x \ln y + \frac{\bar{x}}{x} \ln \bar{x} \ln \bar{y} \right. \\ \left. - \frac{1}{2(x-y)^2} [4\bar{x}^2 x H(x, \bar{y}) + (4x - 5x^2 + y^2)(\ln x + \ln y) \right. \\ \left. + (6x - 5x^2 - 2y + y^2)\bar{x} \frac{\ln \bar{x}}{x} + (2x - 4x^2 + 2y - 4xy + 5x^2 y - y^3) \frac{\ln \bar{y}}{y} \right] \left. \right\}$
A36	$-\frac{1}{3} \left[\eta_{IR} \left(\frac{\bar{x}}{x} \ln \bar{x} + \frac{\bar{y}}{y} \ln \bar{y} \right) + \frac{\bar{x}}{x} \ln \bar{x} + \frac{\bar{y}}{y} \ln \bar{y} + \frac{\bar{x}}{2x} \ln^2 \bar{x} + \frac{\bar{y}}{2y} \ln^2 \bar{y} + \frac{\bar{x} + \bar{y}}{xy} \ln \bar{x} \ln \bar{y} \right]$
A35	$-\frac{1}{24} \left[2\tilde{\eta}_{IR} + \eta_{IR} \left(2 + \frac{1+x}{x} \ln \bar{x} + \frac{1+y}{y} \ln \bar{y} \right) - 2(1-x-y)H(x, y) + \frac{1+x}{x} \ln \bar{x} \right. \\ \left. + \frac{1+y}{y} \ln \bar{y} + \frac{1+x}{2x} \ln^2 \bar{x} + \frac{1+y}{2y} \ln^2 \bar{y} + \frac{\bar{x} + \bar{y}}{xy} \ln \bar{x} \ln \bar{y} \right]$

The function $R(x, y)$ is defined as

$$\begin{aligned}
R(x, y) = & \frac{1}{(x-y)^2} [(2xy - x - y)(\ln x + \ln y) \\
& + (-2xy^2 - 2y^2 + 10xy - 2y - 4x^2) \frac{\ln \bar{y}}{y} \\
& + (-2yx^2 - 2x^2 + 10xy - 2x - 4y^2) \frac{\ln \bar{x}}{x} \\
& - (y\bar{y}^2 + x\bar{x}^2)H(x, \bar{y})] .
\end{aligned} \tag{2.13}$$

The contribution of individual diagrams listed in Table I as well as the total contribution to the $(q_1 \bar{q}_2) + \gamma^* \rightarrow (q_1 \bar{q}_2)$ amplitude given by Eqs. (2.10-2.13) are in complete agreement with the results obtained in Ref. [9].

It is easily seen from Eqs. (2.10-2.13) that in summing up the contributions of all diagrams to the exclusive amplitude $(q_1 \bar{q}_2) + \gamma^* \rightarrow (q_1 \bar{q}_2)$, the originally present soft singularities (double $1/\epsilon_{IR}^2$ poles) cancel out, as required. The final result for the amplitude contains $1/\epsilon_{UV}$ and only simple $1/\epsilon_{IR}$ poles.

We now proceed to treat these poles. The IR poles in (2.10) are such that they can be absorbed into the meson distribution amplitude. As for the UV poles, we renormalize them using the modified minimal-subtraction (\overline{MS}) scheme. This is carried out by stating that α_S appearing in (2.5) is the bare unrenormalized coupling related to the renormalized physical coupling $\alpha_{\overline{MS}}(\mu_R^2)$ by

$$\alpha_S = \alpha_{\overline{MS}}(\mu_R^2) \left[1 - \frac{\alpha_{\overline{MS}}(\mu_R^2)}{\pi} \frac{\beta_0}{4} \left(\frac{1}{\epsilon_{UV}} \right) \right] . \tag{2.14}$$

As a result, we obtain the following expression for the NLO hard-scattering amplitude for the pion form factor:

$$\begin{aligned}
T_H(x, y, Q^2, \mu_R^2, \mu_F^2) = & \alpha_{\overline{MS}}(\mu_R^2) T_H^{(0)}(x, y, Q^2) \\
& \times \left[1 + \frac{\alpha_{\overline{MS}}(\mu_R^2)}{\pi} T_H^{(1)}(x, y, \mu_R^2/Q^2, \mu_F^2/Q^2) \right] ,
\end{aligned} \tag{2.15}$$

where

$$T_H^{(1)}(x, y, \mu_R^2/Q^2, \mu_F^2/Q^2) = f_{UV}(x, y, \mu_R^2/Q^2) + f_{IR}(x, y, \mu_F^2/Q^2) + f_C(x, y) , \tag{2.16}$$

with the functions f_{UV} , f_{IR} , and f_C given by (2.12). It is to be mentioned that the function f_C , unlike the functions f_{UV} and f_{IR} , is not singular for $x, y \rightarrow 0, 1$.

III. EVOLUTIONAL CORRECTIONS TO THE PION DISTRIBUTION AMPLITUDE

The pion distribution amplitude $\Phi(x, \mu_F^2)$ is the basic valence wave function of the pion controlling exclusive pion processes at large momentum transfer. Its shape is not yet accurately known. It has been shown, however, that the leptonic decay $\pi^+ \rightarrow \mu^+ \nu_\mu$ imposes on $\Phi(x, \mu_F^2)$ a constraint of the form

$$\int_0^1 dx \Phi(x, \mu_F^2) = \frac{f_\pi}{2\sqrt{2}n_C} . \tag{3.1}$$

Given the shape of $\Phi(x, \mu_F^2)$, this relation normalizes it for any μ_F^2 . In (3.1), $f_\pi = 0.131$ GeV is the pion decay constant and $n_C (= 3)$ is the number of QCD colors.

Instead of using $\Phi(x, \mu_F^2)$ satisfying (3.1), one usually introduces the distribution amplitude $\phi(x, \mu_F^2)$ normalized to unity,

$$\int_0^1 dx \phi(x, \mu_F^2) = 1 , \tag{3.2}$$

and related to $\Phi(x, \mu_F^2)$ by

$$\Phi(x, \mu_F^2) = \frac{f_\pi}{2\sqrt{2}n_C} \phi(x, \mu_F^2) . \tag{3.3}$$

Although intrinsically nonperturbative, the pion distribution amplitude $\phi(x, \mu_F^2)$ satisfies an evolution equation of the form

$$\mu_F^2 \frac{\partial}{\partial \mu_F^2} \phi(x, \mu_F^2) = \int_0^1 dy V(x, y, \alpha_S(\mu_F^2)) \phi(y, \mu_F^2), \quad (3.4)$$

in which the evolution kernel is calculable in perturbation theory:

$$\begin{aligned} V(x, y, \alpha_S(\mu_F^2)) \\ = \frac{\alpha_S(\mu_F^2)}{4\pi} V_1(x, y) + \left(\frac{\alpha_S(\mu_F^2)}{4\pi} \right)^2 V_2(x, y) + \dots \end{aligned} \quad (3.5)$$

and has been computed in the one- and two-loop approximations using dimensional regularization and the \overline{MS} scheme.

If the distribution amplitude $\phi(x, \mu_0^2)$ can be calculated at an initial momentum scale μ_0^2 , using QCD sum rules [21] or lattice gauge theory [22], then the differential-integral evolution equation (3.4) can be integrated using the moment method to give $\phi(x, \mu_F^2)$ at any momentum scale $\mu_F^2 > \mu_0^2$.

Because of the complicated structure of the two-loop contribution to the evolutional kernel $V_2(x, y)$, only the first few moments of the evolutional kernel have been computed numerically.

Recently, based on the conformal spin expansion and a conformal consistency relation, the analytical result for the evolution of the flavor-nonsinglet meson distribution amplitude has been determined [20].

To the NLO approximation, this, rather complicated solution has the form

$$\phi(x, \mu_F^2) = \phi^{LO}(x, \mu_F^2) + \frac{\alpha_S(\mu_F^2)}{\pi} \phi^{NLO}(x, \mu_F^2), \quad (3.6)$$

where

$$\begin{aligned} \phi^{LO}(x, \mu_F^2) &= x(1-x) \sum_{n=0}^{\infty} ' C_n^{3/2}(2x-1) \frac{4(2n+3)}{(n+1)(n+2)} \\ &\times \left(\frac{\alpha_S(\mu_0^2)}{\alpha_S(\mu_F^2)} \right)^{\gamma_n^{(0)}/\beta_0} \int_0^1 dy C_n^{3/2}(2y-1) \phi^{(0)}(y, \mu_0^2), \end{aligned} \quad (3.7)$$

and

$$\begin{aligned} \phi^{NLO}(x, \mu_F^2) &= x(1-x) \sum_{n=0}^{\infty} ' \left(\frac{\alpha_S(\mu_0^2)}{\alpha_S(\mu_F^2)} \right)^{\gamma_n^{(0)}/\beta_0} \int_0^1 dy C_n^{3/2}(2y-1) \phi^{LO}(y, \mu_0^2) \\ &\left[C_n^{3/2}(2x-1) \frac{(2n+3)}{(n+1)(n+2)} \left(1 - \frac{\alpha_S(\mu_0^2)}{\alpha_S(\mu_F^2)} \right) \left(\frac{\gamma_n^{(1)}}{2\beta_0} + \frac{\beta_1}{\beta_0^2} \gamma_n^{(0)} \right) \right. \\ &\left. + \sum_{k=n+2}^{\infty} ' C_k^{3/2}(2x-1) \frac{2(2k+3)}{(k+1)(k+2)} S_{kn}(\mu_F^2) C_{kn}^{(1)} \right], \end{aligned} \quad (3.8)$$

with abbreviations

$$S_{kn}(\mu_F^2) = \frac{\gamma_k^{(0)} - \gamma_n^{(0)}}{\gamma_k^{(0)} - \gamma_n^{(0)} + \beta_0} \left[1 - \left(\frac{\alpha_S(\mu_0^2)}{\alpha_S(\mu_F^2)} \right)^{1+(\gamma_k^{(0)} - \gamma_n^{(0)})/\beta_0} \right], \quad (3.9)$$

$$C_{kn}^{(1)} = (2n+3) \left[\frac{\gamma_n^{(0)} - \beta_0 + 4C_F A_{kn}}{(k-n)(k+n+3)} + \frac{2C_F(A_{kn} - \psi(k+2) + \psi(1))}{(n+1)(n+2)} \right], \quad (3.10)$$

$$A_{kn} = \psi\left(\frac{k+n+4}{2}\right) - \psi\left(\frac{k-n}{2}\right) + 2\psi(k-n) - \psi(k+2) - \psi(1), \quad (3.11)$$

and \sum' denoting the sum running only over even n , while $C_n^{3/2}(z)$ are Gegenbauer polynomials of order 3/2 and $C_F = 4/3$. In Eqs. (3.7–3.10), $\gamma_n^{(0)}$ are the usual anomalous dimensions

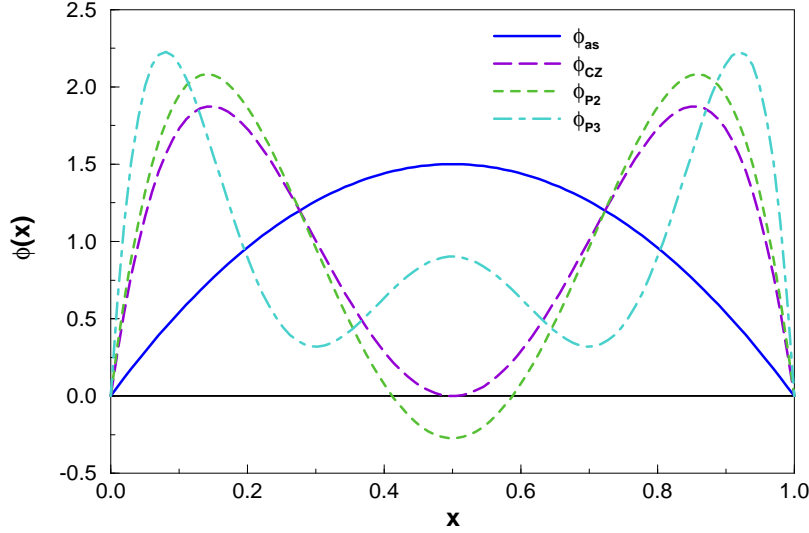


FIG. 4. The four candidate pion distribution amplitudes defined in Eq. (3.16), chosen as nonperturbative inputs at the reference scale $\mu_0^2 = (0.5\text{GeV})^2$.

$$\gamma_n^{(0)} = C_F \left[3 + \frac{2}{(n+1)(n+2)} - 4 \sum_{i=1}^{n+1} \frac{1}{i} \right], \quad (3.12)$$

while β_0 and β_1 are the first two terms in the expansion of the QCD β -function, with β_0 given by (2.3), and

$$\beta_1 = 102 - \frac{38}{3}n_f. \quad (3.13)$$

The function $\psi(z)$ appearing in (3.10) and (3.11) is defined as

$$\psi(z) = \frac{d}{dz}(\ln \Gamma(z)). \quad (3.14)$$

For $n_f = 3$ and for the values of n we are interested in, we have taken the values of the anomalous dimension $\gamma_n^{(1)}$ from [23,24]:

$$\gamma_0^{(1)} = 0, \quad \gamma_2^{(1)} = 111.03, \quad \gamma_4^{(1)} = 150.28. \quad (3.15)$$

For the purpose of our calculation, we use the following four candidate distribution amplitudes (shown in Fig. 4) as nonperturbative inputs at the reference momentum scale $\mu_0^2 = (0.5 \text{ GeV})^2$:

$$\phi_{as}(x) \equiv \phi_{as}(x, \mu_0^2) = 6x(1-x), \quad (3.16a)$$

$$\phi_{CZ}(x) \equiv \phi_{CZ}(x, \mu_0^2) = 6x(1-x) [5(2x-1)^2], \quad (3.16b)$$

$$\phi_{P2}(x) \equiv \phi_{P2}(x, \mu_0^2) = 6x(1-x) [-0.1821 + 5.91(2x-1)^2], \quad (3.16c)$$

$$\phi_{P3}(x) \equiv \phi_{P3}(x, \mu_0^2) = 6x(1-x) [0.6016 - 4.659(2x-1)^2 + 15.52(2x-1)^4]. \quad (3.16d)$$

Here $\phi_{as}(x)$ is the asymptotic distribution amplitude and represents the solution of the evolution equation (3.4) for $\mu_F^2 \rightarrow \infty$. The double-hump-shaped distribution amplitudes $\phi_{CZ}(x)$ and $\phi_{P2}(x)$ and the three-hump-shaped distribution amplitude $\phi_{P3}(x)$ have been obtained using the method of QCD sum rules [21,25]. As Fig. 4 shows, these distribution amplitudes, unlike $\phi_{as}(x)$, are strongly end-point concentrated. In the limit $\mu_F^2 \rightarrow \infty$, they reduce to the asymptotic form $\phi_{as}(x)$.

Owing to the fact that the process we are interested in probes the distribution amplitudes of Eq. (3.16) at the momentum scales $\mu_F^2 \geq \mu_0^2 = (0.5 \text{ GeV})^2$, it is necessary to take into account the evolution of the distribution amplitudes.

On the basis of (3.7) we find that with the LO evolution included, the distribution amplitudes given by (3.16) can generally be written in the form

TABLE II. Coefficients c_0 , c_2 , and c_4 of the general form (3.17) for the candidate distribution amplitudes given by (3.16) with the LO evolution taken into account.

ϕ	c_0	c_2	c_4
ϕ_{as}	1	0	0
ϕ_{CZ}	$1 - \xi^{0.617}$	$5\xi^{0.617}$	0
ϕ_{P2}	$1 - 1.1821\xi^{0.617}$	$5.91\xi^{0.617}$	0
ϕ_{P3}	$1 - 1.1375\xi^{0.617} + 0.7391\xi^{0.899}$	$5.688\xi^{0.617} - 10.347\xi^{0.899}$	$15.52\xi^{0.899}$

$$\phi^{LO}(x, \mu_F^2) = 6x(1-x) [c_0 + c_2(2x-1)^2 + c_4(2x-1)^4], \quad (3.17)$$

with the coefficients c_0 , c_2 , and c_4 listed in Table II, where the notation

$$\xi = \frac{\alpha_S(\mu_F^2)}{\alpha_S(\mu_0^2)}$$

has been introduced.

Next, upon substituting (3.16) at the place of $\phi^{LO}(x, \mu_0^2)$ into Eq. (3.8), we find the NLO evolutional corrections to the distribution amplitude of interest. Results are obtained numerically and cannot be given in a closed form. A summary of our results for the four candidate distribution amplitudes with the NLO evolutional corrections included is shown in Fig. 5. The dash-dotted curves correspond to the distribution amplitudes at the reference point $\mu_F^2 = \mu_0^2 = (0.5 \text{ GeV})^2$. The dashed and solid curves represent the distribution amplitudes evolved to $\mu_F^2 = (2 \text{ GeV})^2$, with the difference that the former includes only LO evolutional corrections, whereas the latter includes NLO evolutional corrections.

IV. CHOOSING THE FACTORIZATION AND THE RENORMALIZATION SCALES

In this section we discuss various possibilities of choosing the renormalization scale μ_R and the factorization scale μ_F appropriate for the process under consideration.

Before entering the discussion, let us now, with the help of Eqs. (1.1), (2.1), and (3.6), write down the complete leading-twist NLO QCD expression for the pion electromagnetic form factor with the μ_R and μ_F dependence of all the terms explicitly indicated.

Generally, for the NLO form factor we can write

$$F_\pi(Q^2, \mu_R^2, \mu_F^2) = F_\pi^{(0)}(Q^2, \mu_R^2, \mu_F^2) + F_\pi^{(1)}(Q^2, \mu_R^2, \mu_F^2). \quad (4.1)$$

The first term in (4.1) is the LO contribution and is given by

$$F_\pi^{(0)}(Q^2, \mu_R^2, \mu_F^2) = \int_0^1 dx \int_0^1 dy \alpha_S(\mu_R^2) \Phi^{LO*}(y, \mu_F^2) T_H^{(0)}(x, y, Q^2) \Phi^{LO}(x, \mu_F^2). \quad (4.2)$$

The second term in (4.1) is the NLO contribution and can be written as

$$F_\pi^{(1)}(Q^2, \mu_R^2, \mu_F^2) = F_\pi^{(1a)}(Q^2, \mu_R^2, \mu_F^2) + F_\pi^{(1b)}(Q^2, \mu_R^2, \mu_F^2), \quad (4.3)$$

where

$$F_\pi^{(1a)}(Q^2, \mu_R^2, \mu_F^2) = \int_0^1 dx \int_0^1 dy \frac{\alpha_S^2(\mu_R^2)}{\pi} \times \Phi^{LO*}(y, \mu_F^2) T_H^{(0)}(x, y, Q^2) T_H^{(1)}(x, y, \mu_R^2/Q^2, \mu_F^2/Q^2) \Phi^{LO}(x, \mu_F^2), \quad (4.4)$$

is the contribution coming from the NLO correction to the hard-scattering amplitude, whereas

$$F_\pi^{(1b)}(Q^2, \mu_R^2, \mu_F^2) = \int_0^1 dx \int_0^1 dy \frac{\alpha_S(\mu_R^2)\alpha_S(\mu_F^2)}{\pi} \times \left[\Phi^{NLO*}(y, \mu_F^2) T_H^{(0)}(x, y, Q^2) \Phi^{LO}(x, \mu_F^2) + \Phi^{LO*}(y, \mu_F^2) T_H^{(0)}(x, y, Q^2) \Phi^{NLO}(x, \mu_F^2) \right], \quad (4.5)$$

is the contribution arising from the inclusion of the NLO evolution of the distribution amplitude. Now, if (2.4) is taken into account, the expression for the LO contribution of Eq. (4.2) can be written in the form

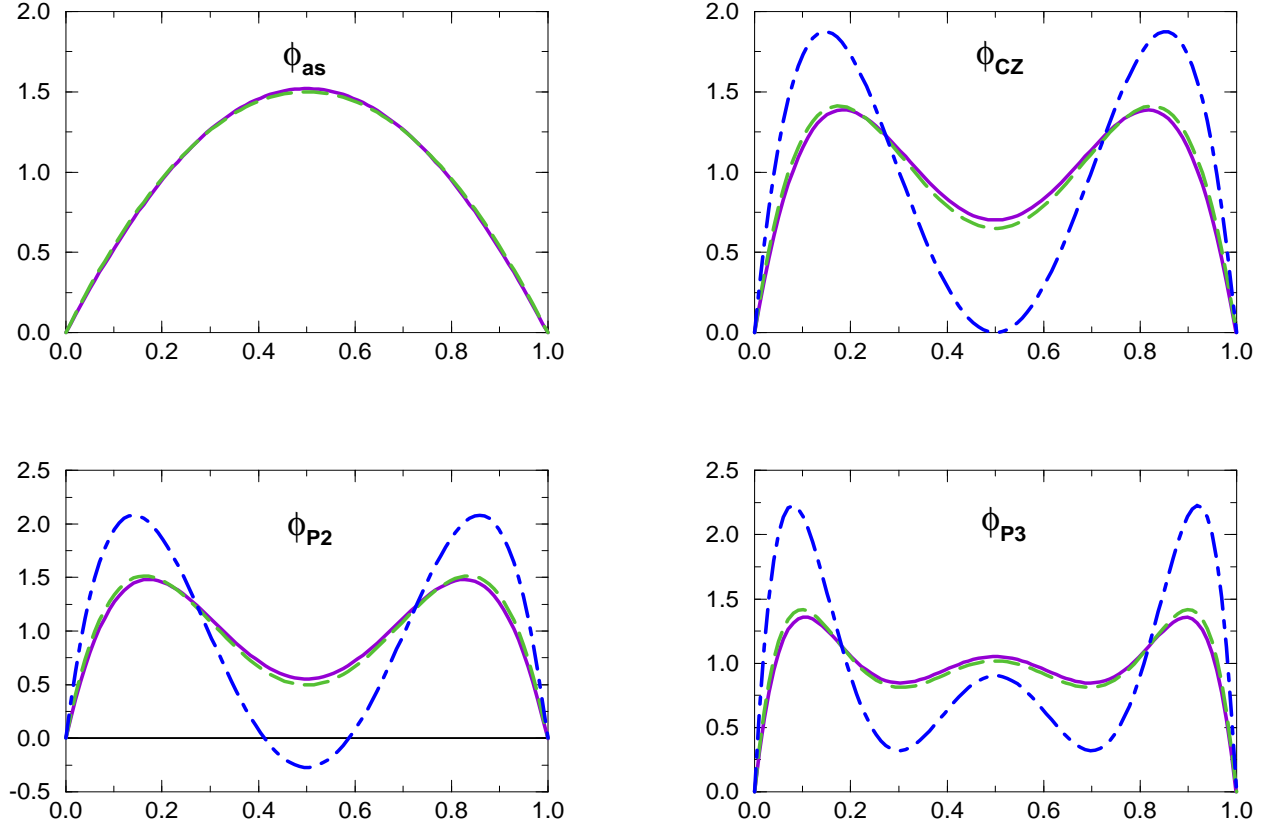


FIG. 5. Evolution of the four candidate pion distribution amplitudes: $\phi_{as}(x, \mu_F^2)$, $\phi_{CZ}(x, \mu_F^2)$, $\phi_{P2}(x, \mu_F^2)$, and $\phi_{P3}(x, \mu_F^2)$, with running coupling constant $\alpha_S(\mu_F^2)$ and three active flavors. The dash-dotted curves correspond to the distribution amplitudes given by (3.16) and taken as nonperturbative input at the reference momentum scale $\mu_0^2 = (0.5 \text{ GeV})^2$. The dashed curves correspond to the distribution amplitudes at the momentum scale $\mu_F^2 = (2 \text{ GeV})^2$ with the LO evolutionary corrections included according to (3.17) and Table II. The solid curves correspond to the distribution amplitudes at the momentum scale $\mu_F^2 = (2 \text{ GeV})^2$ with the NLO evolutionary corrections taken into account according to Eqs. (3.6–3.8).

$$F_\pi^{(0)}(Q^2, \mu_R^2, \mu_F^2) = \frac{8}{9} \pi \frac{f_\pi^2}{Q^2} \int_0^1 dx \int_0^1 dy \quad \alpha_S(\mu_R^2) \frac{\phi^{LO}(x, \mu_F^2)}{\bar{x}} \frac{\phi^{LO*}(y, \mu_F^2)}{\bar{y}}. \quad (4.6)$$

Next, before going on to perform the remaining x and y integrations, we have to choose the renormalization scale μ_R and the factorization scale μ_F . In doing this, however, there is considerable freedom involved.

The physical pion form factor $F_\pi(Q^2)$, represented at the sufficiently high Q^2 by the factorization formula (1.1), is independent of the renormalization scheme and the renormalization and factorization scales, μ_R and μ_F . Truncation of the perturbative series of $F_\pi(Q^2)$ at any finite order causes a residual dependence on the scheme as well as on the scales.

We approximate $F_\pi(Q^2)$ only by two terms of the perturbative series and hope that we can minimize higher-order corrections by a suitable choice of μ_R and μ_F , so that the LO term $F_\pi^{(0)}(Q^2, \mu_R^2, \mu_F^2)$ gives a good approximation to the complete sum $F_\pi(Q^2)$.

It should be noted that in $F_\pi^{(0)}(Q^2, \mu_R^2, \mu_F^2)$, given by (4.2), μ_R appears only through $\alpha_S(\mu_R^2)$, whereas μ_F enters into the distribution amplitude $\phi(x, \mu_F^2)$. In $F_\pi^{(1)}(Q^2, \mu_R^2, \mu_F^2)$, given by (4.3–4.5), a logarithmic dependence on the scales μ_R and μ_F appears through $T_H^{(1)}(x, y, \mu_R^2/Q^2, \mu_F^2/Q^2)$. As it is seen from (2.12) and (2.16), this dependence is contained in the terms

$$f_{UV}(x, y, Q^2/\mu_R^2) = \frac{1}{4} \beta_0 \left[\frac{2}{3} - \ln(\bar{x}\bar{y}) + \ln \frac{\mu_R^2}{Q^2} \right], \quad (4.7)$$

$$f_{IR}(x, y, Q^2/\mu_F^2) = \frac{2}{3} [3 + \ln(\bar{x}\bar{y})] \left[\frac{1}{2} \ln(\bar{x}\bar{y}) - \ln \frac{\mu_F^2}{Q^2} \right]. \quad (4.8)$$

Being independent of each other, the scales μ_R and μ_F can be expressed in terms of Q^2 as

$$\mu_R^2 = a(x, y) Q^2, \quad (4.9)$$

$$\mu_F^2 = b(x, y) Q^2, \quad (4.10)$$

where $a(x, y)$ and $b(x, y)$ are some linear functions of the dimensionless variables x and y (quark longitudinal momentum fractions). A consequence of this is that the model distribution amplitude enters into these scales, making it impossible for them to be consistently set for all possible distributions.

We next discuss various possibilities of choosing the scales μ_R and μ_F separately. The simplest and widely used choice for the scale μ_R is

$$\mu_R^2 = Q^2, \quad (4.11)$$

the justification for the use of which is mainly pragmatic.

Physically, however, the more appropriate choice for μ_R^2 would be the one corresponding to the characteristic virtualities of the particles in the parton subprocess, which is considerably lower than the overall momentum transfer Q^2 (i.e., virtuality of the probing photon). It follows from Figs. 1 and 2 that the virtualities of the gluon line (line 4) and the internal quark line (line 2) of diagram A in Fig. 2 are given by $\bar{x}\bar{y}Q^2$ and $\bar{y}Q^2$, respectively. Now, if instead of using (4.11) we choose μ_R to be equal to the gluon virtuality, i.e.,

$$\mu_R^2 = \bar{x}\bar{y}Q^2, \quad (4.12)$$

then the logarithmic terms in (4.7) vanish.

As it is well known, unlike in an Abelian theory (e.g., QED), where the effective coupling is entirely renormalized by the corrections of the vector particle propagator, in QCD the coupling is renormalized not only by the gluon propagator, but also by the quark-gluon vertex and quark propagator corrections. It is thus possible to choose μ_R^2 as the geometrical mean of the gluon and quark virtualities [6]:

$$\mu_R^2 = \sqrt{(\bar{x}\bar{y}Q^2)(\bar{y}Q^2)}. \quad (4.13)$$

Alternatively, we can make a choice

$$\mu_R^2 = e^{-2/3} \bar{x}\bar{y}Q^2, \quad (4.14)$$

as a result of which the function f_{UV} , given by (4.7), vanishes identically. In this case, $T_H^{(1)}(x, y, \mu_R^2/Q^2, \mu_F^2/Q^2)$ defined by (2.16) becomes n_f independent. This is an example of choosing the renormalization scale according to the Brodsky-Lepage-Mackenzie (BLM) procedure [26]. In this procedure, the renormalization scale μ_R^2 best suited to a particular process in a given order can be determined by computing vacuum-polarization insertions in the diagrams

of that order. The essence of the BLM procedure is that all vacuum-polarization effects from the QCD β function are resummed into the running coupling constant.

As for the factorization scale μ_F^2 , a natural choice would be

$$\mu_F^2 = Q^2, \quad (4.15)$$

which eliminates the logarithms of Q^2/μ_F^2 . More preferable to (4.15) is the choice

$$\mu_F^2 = \sqrt{\bar{x}\bar{y}} Q^2, \quad (4.16)$$

which makes the function f_{IR} , given by (4.8), vanish.

A glance at Eqs. (4.1–4.5), where the coupling constants $\alpha_S(\mu_R^2)$ and $\alpha_S(\mu_F^2)$ appear under the integral sign, reveals that any of the choices of μ_R given by (4.12–4.14), and the choice of μ_F given by (4.16), leads immediately to the problem if the usual one-loop formula (2.2) for the effective QCD running coupling constant is employed. Namely, then, regardless of how large Q^2 is, the integration of Eqs. (4.1–4.5) allows $\alpha_S(\mu_R^2)$ to be evaluated near zero momentum transfer. Two approaches are possible to circumvent this problem. First, one can choose μ_R^2 and μ_F^2 to be effective constants by taking $\mu_R^2 = \langle \mu_R^2 \rangle$ and $\mu_F^2 = \langle \mu_F^2 \rangle$, respectively. Second, one can introduce a cutoff in formula (2.2) with the aim of preventing the effective coupling from becoming infinite for vanishing gluon momenta.

If the first approach is taken, Eqs. (4.12–4.14) and (4.16) get replaced by the averages

$$\mu_R^2 = \langle \bar{x}\bar{y} Q^2 \rangle, \quad (4.17)$$

$$\mu_R^2 = \sqrt{\langle \bar{x}\bar{y} Q^2 \rangle \langle \bar{y} Q^2 \rangle}, \quad (4.18)$$

$$\mu_R^2 = \left\langle e^{-2/3} \bar{x}\bar{y} Q^2 \right\rangle, \quad (4.19)$$

and

$$\mu_F^2 = \sqrt{\langle \bar{x}\bar{y} \rangle} Q^2, \quad (4.20)$$

respectively. Taking into account the fact that $\langle \bar{x}\bar{y} \rangle = \langle \bar{x} \rangle \langle \bar{y} \rangle$ and $\langle \bar{x} \rangle = \langle \bar{y} \rangle$, it is possible to write Eqs. (4.17–4.20) in the respective forms:

$$\mu_R^2 = \langle \bar{x} \rangle^2 Q^2, \quad (4.21)$$

$$\mu_R^2 = \langle \bar{x} \rangle^{3/2} Q^2, \quad (4.22)$$

$$\mu_R^2 = e^{-2/3} \langle \bar{x} \rangle^2 Q^2, \quad (4.23)$$

and

$$\mu_F^2 = \langle \bar{x} \rangle Q^2. \quad (4.24)$$

The key quantity in the above considerations is $\langle \bar{x} \rangle$, the average value of the momentum fraction. It depends on the form of the distribution amplitude, and there is no unique way of defining it. A possible definition is

$$\langle \bar{x} \rangle (\mu_F^2) = \frac{\int \bar{x} \phi(x, \mu_F^2) dx}{\int \phi(x, \mu_F^2) dx}. \quad (4.25)$$

Owing to the fact that all the distribution amplitudes under consideration are centered around the value $x = 0.5$, it follows trivially from (4.25) that

$$\langle \bar{x} \rangle (\mu_F^2) = \langle \bar{x} \rangle_{as} (\mu_F^2) = \langle \bar{x} \rangle_{CZ} (\mu_F^2) = \langle \bar{x} \rangle_{P_2} (\mu_F^2) = \langle \bar{x} \rangle_{P_3} (\mu_F^2) = 0.5. \quad (4.26)$$

An alternative way of defining $\langle \bar{x} \rangle$, motivated by the form of the LO expression for the pion form factor (4.6), is

$$\langle \bar{x} \rangle (\mu_F^2) = \frac{\int \bar{x} \frac{\phi^{LO}(x, \mu_F^2)}{\bar{x}} dx}{\int \frac{\phi^{LO}(x, \mu_F^2)}{\bar{x}} dx}. \quad (4.27)$$

It should be noted, however, that this formula can be straightforwardly applied only if $\mu_F^2 = Q^2$. The values of $\langle \bar{x} \rangle$ obtained for the four pion distribution amplitudes are listed in Table III. On the other hand, if instead of $\mu_F^2 = Q^2$

TABLE III. Variation with Q^2 of the average value of the momentum fraction, $\langle \bar{x} \rangle (Q^2)$, as defined by Eq. (4.27), for the four candidate distributions given by (3.17).

Q^2	$\langle \bar{x} \rangle (Q^2)$			
	ϕ_{as}	ϕ_{CZ}	ϕ_{P2}	ϕ_{P3}
0.25	0.333	0.200	0.186	0.155
4	0.333	0.242	0.230	0.208
5	0.333	0.244	0.233	0.211
6	0.333	0.245	0.234	0.213
7	0.333	0.247	0.235	0.214
8	0.333	0.248	0.237	0.216
9	0.333	0.248	0.237	0.217
10	0.333	0.249	0.238	0.218
20	0.333	0.254	0.243	0.224
30	0.333	0.256	0.246	0.227
40	0.333	0.258	0.247	0.229
50	0.333	0.259	0.249	0.231
100	0.333	0.262	0.252	0.235

one chooses the factorization scale to be as given by (4.24), then Eqs. (4.24) and (4.27) form a nontrivial system of simultaneous equations.

As we have seen above, the divergence of the effective QCD coupling $\alpha_S(\mu_R^2)$, as given by (2.2), for $\mu_R^2 \rightarrow 0$, is the reason that it is not possible to use the choices of μ_R^2 given by (4.12–4.14) and μ_F^2 given by (4.16). Equation (2.2) is not an accurate representation of $\alpha_S(\mu_R^2)$ for small μ_R^2 , and a number of proposals have been suggested for the form of $\alpha_S(\mu_R^2)$ in this regime [27]. In this work we adopt the following simple parametrization for the effective QCD coupling proposed by Cornwall [27]:

$$\alpha_S(\mu_R^2) = \frac{4\pi}{\beta_0 \ln \left(\frac{\mu_R^2 + 4m_g^2}{\Lambda^2} \right)}, \quad (4.28)$$

where m_g is interpreted as an “effective dynamical gluon mass”. For $\mu_R^2 \gg m_g^2$, the effective coupling in (4.28) coincides with the one-loop formula (2.2), whereas at low momentum transfer this formula “freezes” to some finite but not necessarily small value.

With the frozen coupling constant formula (4.28), the choices of the renormalization and factorization scales, μ_R^2 and μ_F^2 , given by Eqs. (4.12–4.14) and (4.16), respectively, become viable options, and the NLO expression for the form factor given by (4.1–4.5) can be directly integrated.

V. COMPLETE NLO NUMERICAL PREDICTIONS FOR THE PION FORM FACTOR

Having obtained all the necessary ingredients in the preceding sections, now we put them together and obtain complete leading-twist NLO QCD numerical predictions for the pion form factor. For fixed distribution amplitude, we analyze the dependence of our results on the choice of the scales μ_R and μ_F .

We take that a perturbative prediction for $F_\pi(Q^2)$ can be considered reliable provided the following two requirements are met: first, corrections to the LO prediction are reasonably small ($< 30\%$); second, the expansion parameter (effective QCD coupling constant) is acceptably small (< 0.3). Of course, one more requirement should be added to the above ones: consistency with the experimental data. This requirement, however, is not of much use here since reliable experimental data for the pion form factor exist for $Q^2 \leq 4 \text{ GeV}^2$, i.e., well outside the region in which the perturbative treatment based on Eq. (1.1) is justified.

Based on the above requirements we adopt the standard according to which a prediction is considered reliable for the values of Q^2 such that $Q^2 > \max(Q_1^2, Q_2^2)$, where Q_1^2 and Q_2^2 are the values of Q^2 at which given prediction meets the first and the second requirement, respectively. It turns out that these two requirements are rather restrictive (especially the second one) so that in all the cases considered we find that $\max(Q_1^2, Q_2^2)$ is large enough to justify the perturbative treatment. Given two predictions A and B , obtained with the same distribution amplitude, but corresponding to two different choices of scales μ_R^2 and μ_F^2 , reliable (in the above sense) for momentum transfer $Q^2 > Q_A^2$ and $Q^2 > Q_B^2$, respectively, the prediction A will be considered “better” if $Q_A^2 < Q_B^2$.

In order to estimate the dependence of our results to the contribution of the end-point region (soft physics) we examine to what extent they are modified if use is made of the assumption of the frozen coupling constant at low momentum transfer (4.28).

A. Predictions obtained with $\mu_R^2 = \mu_F^2 = Q^2$

In order to compare our results with some of those obtained previously, we first calculate the NLO prediction for $Q^2 F_\pi(Q^2)$ with the evolution of the distribution amplitude completely neglected. Using the \overline{MS} scheme and with $\mu_R^2 = \mu_F^2 = Q^2$, we find that the perturbative series for $Q^2 F_\pi(Q^2)$ corresponding to the four candidate distribution amplitudes, given by (3.16), look like

$$\phi_{as}(x) : \quad Q^2 F_\pi(Q^2) = (0.43 \text{ GeV}^2) \alpha_S(Q^2) [1 + 1.38 \alpha_S(Q^2) + \dots], \quad (5.1)$$

$$\phi_{CZ}(x) : \quad Q^2 F_\pi(Q^2) = (1.20 \text{ GeV}^2) \alpha_S(Q^2) [1 + 2.69 \alpha_S(Q^2) + \dots], \quad (5.2)$$

$$\phi_{P2}(x) : \quad Q^2 F_\pi(Q^2) = (1.38 \text{ GeV}^2) \alpha_S(Q^2) [1 + 2.84 \alpha_S(Q^2) + \dots], \quad (5.3)$$

$$\phi_{P3}(x) : \quad Q^2 F_\pi(Q^2) = (2.00 \text{ GeV}^2) \alpha_S(Q^2) [1 + 3.67 \alpha_S(Q^2) + \dots]. \quad (5.4)$$

Thus, as it is seen from the above expressions, the LO result as well as the NLO correction to the pion form factor increase when one moves from the least end-point concentrated distribution amplitude $\phi_{as}(x)$ to the most end-point concentrated one $\phi_{P3}(x)$.

The first NLO prediction for the pion form factor was obtained in Ref. [5]. Using the \overline{MS} renormalization scheme and the choice $\mu_R^2 = \mu_F^2 = Q^2$ it was found that for the asymptotic distribution amplitude, given by (3.16), the perturbative series took the form

$$Q^2 F_\pi(Q^2) = (0.43 \text{ GeV}^2) \alpha_S(Q^2) [1 + 2.1 \alpha_S(Q^2) + \dots]. \quad (5.5)$$

The conclusion based on this result was that a reliable result for $F_\pi(Q^2)$ was not obtained until $\alpha_S(Q^2) \approx 0.1$, or with $\Lambda_{\overline{MS}} = 0.5 \text{ GeV}$, $Q^2 = 10000 \text{ GeV}^2$. This prediction has been widely cited in the literature and initiated a lot of discussion regarding the applicability of PQCD to the calculation of exclusive processes at large-momentum transfer. In spite of the fact that some serious mistakes in the analytical results for the hard-scattering amplitude were pointed out [9], a complete numerical revision, to the best of our knowledge, has not been reported yet.

Since, according to (2.2), $Q^2 = 10000 \text{ GeV}^2$ implies $\alpha_S(Q^2) = 0.13$, it follows from (5.5) that $F_\pi^{(1)}(Q^2)/F_\pi^{(0)}(Q^2) \approx 0.28$. On the other hand, if use is made of (5.1), with $\Lambda_{\overline{MS}} = 0.5 \text{ GeV}$, it is easily seen that the ratio $F_\pi^{(1)}(Q^2)/F_\pi^{(0)}(Q^2) \approx 0.28$ is achieved already for $Q^2 \approx 260 \text{ GeV}^2$. Taking the presently accepted value of 0.2 GeV for $\Lambda_{\overline{MS}}$ gives a still lower value of Q^2 , namely, $Q^2 \approx 40 \text{ GeV}^2$.

Thus, on the basis of (5.1) we find that a reliable prediction for $F_\pi(Q^2)$ can be obtained at $Q^2 \approx 40 \text{ GeV}^2$! It should be pointed out once more that this prediction has been obtained by neglecting the contribution due to the evolution of the distribution amplitude.

Currently available experimental data for the spacelike pion electromagnetic form factor $F_\pi(Q^2)$ are shown in Fig. 6. The data are taken from Bebek et al. [29] and Amendolia et al. [30]. As stated in [29], the measurements corresponding to $Q^2 = 6.30 \text{ GeV}^2$ and $Q^2 = 9.77 \text{ GeV}^2$ are somewhat questionable. Thus, effectively, the data for $F_\pi(Q^2)$ exist only for Q^2 in the range $Q^2 \leq 4 \text{ GeV}^2$. The results of Ref. [29] were obtained from the extrapolation of the $\gamma^* p \rightarrow \pi^+ n$ electroproduction data to the pion pole. It should also be mentioned that the analysis of Ref. [29] is subject to criticism which questions whether $F_\pi(Q^2)$ was truly determined for $1 \leq Q^2 \leq 4 \text{ GeV}^2$ [31] (but see also Ref. [32]).

Next, we present the NLO results obtained with the evolution of the distribution amplitude incorporated.

With the evolution of the distribution amplitudes included, it is no longer possible to represent the NLO prediction in the form of a perturbative series similar to those in Eqs. (5.1–5.4). Namely, in this case, the coefficients of the perturbative series depend on Q^2 , which is due to the Q^2 dependence of the evolutional correction to the distribution amplitude. Numerical results of our complete NLO QCD calculation of the “almost scaling” combination $Q^2 F_\pi(Q^2)$, obtained using the four candidate distribution amplitudes, with $\mu_R^2 = \mu_F^2 = Q^2$, and for $Q^2 \geq 4 \text{ GeV}^2$, are displayed in Tables IV, V, VI, and VII. The entries in these tables include various contributions defined by Eqs. (4.1–4.5) comprising the full NLO result. A comparison of our results with presently available experimental data is shown in Fig. 7. The ratio of the NLO to the LO contribution to $F_\pi(Q^2)$, i.e., $F_\pi^{(1)}(Q^2)/F_\pi^{(0)}(Q^2)$, as a useful measure of the importance of the NLO corrections, is plotted as a function of Q^2 in Fig. 8. The shaded areas appearing in Figs. 7 and 8 denote the region of Q^2 where $\alpha_S(Q^2) > 0.3$. We take that outside of this region the effective coupling is acceptably small.

It is evident from Figs. 7 and 8 and Tables IV–VII that the leading-twist NLO results for the pion form factor obtained with $\mu_R^2 = \mu_F^2 = Q^2$ display the following general features. First, the results are quite sensitive to the

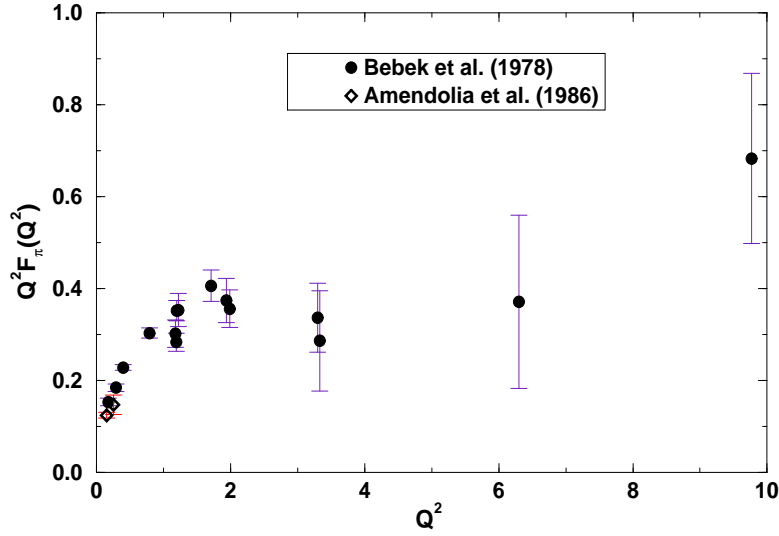


FIG. 6. Presently available experimental data for the spacelike pion electromagnetic form factor.

TABLE IV. Complete leading-twist NLO QCD results for the pion form factor, $Q^2 F_\pi(Q^2)$, obtained using the $\phi_{as}(x, \mu_F^2)$ distribution amplitude and assuming $\mu_R^2 = \mu_F^2 = Q^2$.

Q^2	$\alpha_S(\mu_R^2)$	$Q^2 F_\pi^{(0)}(Q^2)$	$Q^2 F_\pi^{(1a)}(Q^2)$	$Q^2 F_\pi^{(1b)}(Q^2)$	$Q^2 F_\pi^{(1)}(Q^2)$	$F_\pi^{(1)}(Q^2)/F_\pi^{(0)}(Q^2)$	$Q^2 F_\pi(Q^2)$
4	0.303	0.131	0.055	-0.003	0.052	0.397	0.183
5	0.289	0.125	0.050	-0.003	0.047	0.377	0.172
6	0.279	0.120	0.046	-0.003	0.044	0.363	0.164
7	0.270	0.117	0.044	-0.003	0.041	0.351	0.158
8	0.264	0.114	0.041	-0.003	0.039	0.341	0.153
9	0.258	0.111	0.040	-0.003	0.037	0.334	0.148
10	0.253	0.109	0.038	-0.003	0.036	0.327	0.145
20	0.225	0.097	0.030	-0.002	0.028	0.288	0.125
30	0.211	0.091	0.027	-0.002	0.025	0.268	0.115
40	0.202	0.087	0.024	-0.002	0.022	0.257	0.110
50	0.196	0.085	0.023	-0.002	0.021	0.248	0.105
100	0.178	0.077	0.019	-0.002	0.017	0.225	0.094

TABLE V. Same as Table IV but for the $\phi_{CZ}(x, \mu_F^2)$ distribution amplitude.

Q^2	$\alpha_S(\mu_R^2)$	$Q^2 F_\pi^{(0)}(Q^2)$	$Q^2 F_\pi^{(1a)}(Q^2)$	$Q^2 F_\pi^{(1b)}(Q^2)$	$Q^2 F_\pi^{(1)}(Q^2)$	$F_\pi^{(1)}(Q^2)/F_\pi^{(0)}(Q^2)$	$Q^2 F_\pi(Q^2)$
4	0.303	0.248	0.169	-0.016	0.152	0.614	0.401
5	0.289	0.233	0.150	-0.016	0.134	0.576	0.367
6	0.279	0.222	0.136	-0.015	0.122	0.548	0.343
7	0.270	0.213	0.126	-0.014	0.112	0.526	0.325
8	0.264	0.206	0.119	-0.014	0.105	0.508	0.311
9	0.258	0.200	0.112	-0.014	0.099	0.493	0.299
10	0.253	0.195	0.107	-0.013	0.094	0.481	0.289
20	0.225	0.167	0.080	-0.011	0.069	0.409	0.236
30	0.211	0.154	0.068	-0.010	0.058	0.376	0.212
40	0.202	0.146	0.062	-0.010	0.052	0.354	0.198
50	0.196	0.140	0.057	-0.009	0.048	0.339	0.188
100	0.178	0.125	0.045	-0.008	0.037	0.298	0.162

TABLE VI. Same as Table IV but for the $\phi_{P2}(x, \mu_F^2)$ distribution amplitude.

Q^2	$\alpha_S(\mu_R^2)$	$Q^2 F_\pi^{(0)}(Q^2)$	$Q^2 F_\pi^{(1a)}(Q^2)$	$Q^2 F_\pi^{(1b)}(Q^2)$	$Q^2 F_\pi^{(1)}(Q^2)$	$F_\pi^{(1)}(Q^2)/F_\pi^{(0)}(Q^2)$	$Q^2 F_\pi(Q^2)$
4	0.303	0.274	0.196	-0.020	0.176	0.644	0.450
5	0.289	0.256	0.173	-0.019	0.155	0.604	0.411
6	0.279	0.244	0.158	-0.018	0.140	0.574	0.384
7	0.270	0.234	0.146	-0.017	0.129	0.551	0.363
8	0.264	0.226	0.137	-0.017	0.120	0.532	0.346
9	0.258	0.219	0.129	-0.016	0.113	0.517	0.332
10	0.253	0.214	0.123	-0.016	0.107	0.503	0.321
20	0.225	0.182	0.091	-0.013	0.078	0.428	0.260
30	0.211	0.168	0.078	-0.012	0.066	0.392	0.233
40	0.202	0.158	0.070	-0.012	0.058	0.369	0.217
50	0.196	0.152	0.065	-0.011	0.054	0.353	0.205
100	0.178	0.135	0.051	-0.010	0.042	0.310	0.176

TABLE VII. Same as Table IV but for the $\phi_{P3}(x, \mu_F^2)$ distribution amplitude.

Q^2	$\alpha_S(\mu_R^2)$	$Q^2 F_\pi^{(0)}(Q^2)$	$Q^2 F_\pi^{(1a)}(Q^2)$	$Q^2 F_\pi^{(1b)}(Q^2)$	$Q^2 F_\pi^{(1)}(Q^2)$	$F_\pi^{(1)}(Q^2)/F_\pi^{(0)}(Q^2)$	$Q^2 F_\pi(Q^2)$
4	0.303	0.675	0.544	-0.400	0.144	0.213	0.819
5	0.289	0.612	0.468	-0.356	0.112	0.183	0.724
6	0.279	0.568	0.416	-0.325	0.091	0.161	0.659
7	0.270	0.534	0.378	-0.301	0.077	0.144	0.611
8	0.264	0.507	0.349	-0.283	0.066	0.130	0.573
9	0.258	0.485	0.326	-0.268	0.058	0.119	0.543
10	0.253	0.467	0.307	-0.256	0.051	0.110	0.518
20	0.225	0.370	0.212	-0.191	0.022	0.058	0.391
30	0.211	0.327	0.175	-0.163	0.012	0.035	0.339
40	0.202	0.302	0.154	-0.147	0.007	0.022	0.308
50	0.196	0.284	0.140	-0.136	0.003	0.012	0.288
100	0.178	0.239	0.105	-0.108	-0.003	-0.012	0.237

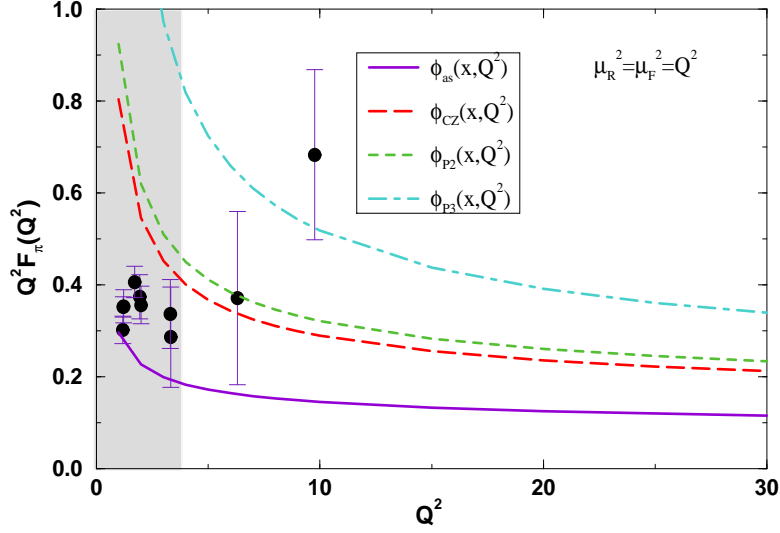


FIG. 7. Comparison of the complete leading-twist NLO QCD predictions for the pion form factor, $Q^2 F_\pi(Q^2)$, obtained using the four candidate distribution amplitudes, with the presently available experimental data. The shaded area denotes the region of Q^2 in which $\alpha_S(Q^2) > 0.3$.

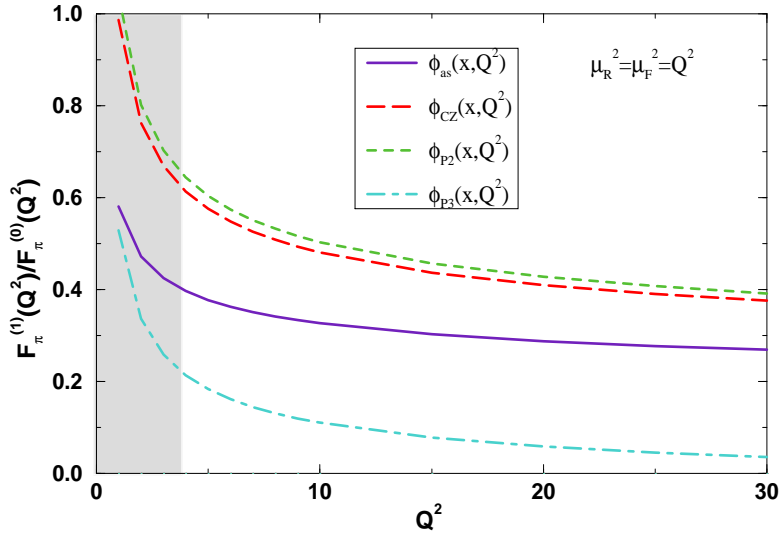


FIG. 8. The ratio of the NLO to the LO contributions to the pion form factor, $F_\pi^{(1)}(Q^2)/F_\pi^{(0)}(Q^2)$, for the four candidate distribution amplitudes. The shaded area denotes the region of Q^2 in which $\alpha_S(Q^2) > 0.3$.

assumed form of the pion distribution amplitude. Thus, the more end-point concentrated distribution amplitude is, the larger result is obtained for the pion form factor. Second, the distribution amplitudes $\phi_{CZ}(x, \mu_F^2)$ and $\phi_{P2}(x, \mu_F^2)$ lead to very similar predictions. Third, the data are located in the range of the predictions obtained by using the $\phi_{as}(x, Q^2)$ and $\phi_{CZ}(x, Q^2)$ distributions. Fourth, whereas the NLO correction arising from corrections to the hard-scattering amplitude are positive, corrections due to inclusion of the evolutional corrections to the distribution amplitude are negative, with the former being generally an order of magnitude larger than the latter with the exception of the $\phi_{P3}(x, \mu_F^2)$ distribution for which both contributions comprising the NLO corrections are of the same order of magnitude. Thus, in all the cases considered the full NLO correction to the pion form factor is positive, i.e., its inclusion increases the LO prediction.

We now briefly comment on the results obtained with each of the four distribution amplitudes. Table IV, which corresponds to the $\phi_{as}(x, Q^2)$ distribution amplitude, shows that the NLO correction, $Q^2 F_\pi^{(1)}(Q^2)$, is reasonably small (less than 30%) for $Q^2 > 15 \text{ GeV}^2$. Also, the contribution to $Q^2 F_\pi^{(1)}(Q^2)$ due to the inclusion of the NLO evolutional correction to the distribution amplitude, $Q^2 F_\pi^{(1b)}(Q^2)$, is rather small (of order 2%). As it is seen from Fig. 7 as well as from Table IV, the LO result $Q^2 F_\pi^{(0)}(Q^2)$ is lower than the experimental value by roughly a factor of three, whereas the full NLO result is lower by a factor of two.

The results derived from the $\phi_{CZ}(x, Q^2)$ distribution are presented in Table V. The full NLO correction $Q^2 F_\pi^{(1)}(Q^2)$ is somewhat larger than for $\phi_{as}(x, Q^2)$, and at $Q^2 \approx 100 \text{ GeV}^2$ it amounts to less than 30%. It is important to observe that the evolutional corrections, especially the LO ones, are in this case rather significant. Thus, if the results given in Table V are compared with those following from Eq. (5.2), one finds that the LO result $Q^2 F_\pi^{(0)}(Q^2)$ obtained with $\phi_{CZ}^{LO}(x, Q^2)$ is considerably lower than that obtained with $\phi_{CZ}(x)$. As it is seen from Table V, the NLO evolutional correction $Q^2 F_\pi^{(1b)}(Q^2)$ is of order $\approx 7\%$, i.e., nonnegligible. To show the importance of the correction arising from the inclusion of the distribution amplitude evolution, the results for $Q^2 F_\pi(Q^2)$ and the ratio $F_\pi^{(1)}(Q^2)/F_\pi^{(0)}(Q^2)$ obtained using the $\phi_{CZ}(x)$, $\phi_{CZ}^{LO}(x, Q^2)$, and $\phi_{CZ}(x, Q^2)$ distributions, are exhibited in Figs. 9 and 10, respectively. As Fig. 7 shows, the predictions obtained with the $\phi_{CZ}(x, Q^2)$ distribution are in fair agreement with the existing data.

The results based on the $\phi_{P2}(x, Q^2)$ distribution are listed in Table VI. This distribution, however, offers nothing new. Namely, as it can easily be seen by looking at Figs. 7 and 8 and by comparing the corresponding entries in Tables V and VI, the results obtained with the $\phi_{P2}(x, Q^2)$ and $\phi_{CZ}(x, Q^2)$ distributions are practically the same qualitatively, while differ quantitatively by a few percent. For this reason, we leave the $\phi_{P2}(x, Q^2)$ distribution out of our further consideration.

Finally, the results with the $\phi_{P3}(x, \mu_F^2)$ distribution are summarized in Table VII. It is evident from this table and Fig. 7 that the predictions obtained with this distribution are substantially larger and overshoot the data markedly, and as such it can safely be ruled out.

In view of what has been said above we may conclude the following. Of the four distribution amplitudes considered only two appear to be relevant, namely, $\phi_{as}(x, \mu_F^2)$ and $\phi_{CZ}(x, \mu_F^2)$. They both lead to the predictions which are consistent with the data. In spite of the fact that the results calculated using $\phi_{CZ}(x, \mu_F^2)$ are closer to the data, the quality, quantity, and the region of Q^2 in which the data exist are such that there is nothing indicating in a compelling way why the $\phi_{as}(x, \mu_F^2)$ distribution should (at this point) be excluded. It is worth mentioning here that the theoretical predictions for the photon-to-pion transition form factor $F_{\pi\gamma}(Q^2)$ are in very good agreement with the data assuming the pion distribution amplitude is close to the asymptotic one, i.e., $\phi_{as}(x, \mu_F^2)$ [33].

B. Predictions obtained using $\mu_R^2 = a Q^2$ and $\mu_F^2 = b Q^2$

In the following we restrict our attention only to the $\phi_{as}(x, \mu_F^2)$ and $\phi_{CZ}(x, \mu_F^2)$ distribution amplitudes. In the preceding subsection we have found that the NLO corrections to these two distributions are large, especially for the latter. The reason is that the renormalization scale choice $\mu_R^2 = Q^2$ is inappropriate. Namely, owing to the partitioning of the overall momentum transfer Q^2 among the particles in the parton subprocess, the essential virtualities of the particles are smaller than Q^2 , so that the “physical” renormalization scale, better suited for the process of interest, is inevitably lower than Q^2 .

In this subsection we present our numerical results for the pion form factor for the two distribution amplitudes, and for the choices of the scales μ_R and μ_F given by Eqs. (4.21–4.23) and (4.24), respectively. For a given distribution amplitude and a fixed pair of scales (μ_R, μ_F) , we examine the dependence of the results on the definitions (4.25) and (4.27) of the average momentum fraction $\langle \bar{x} \rangle$.

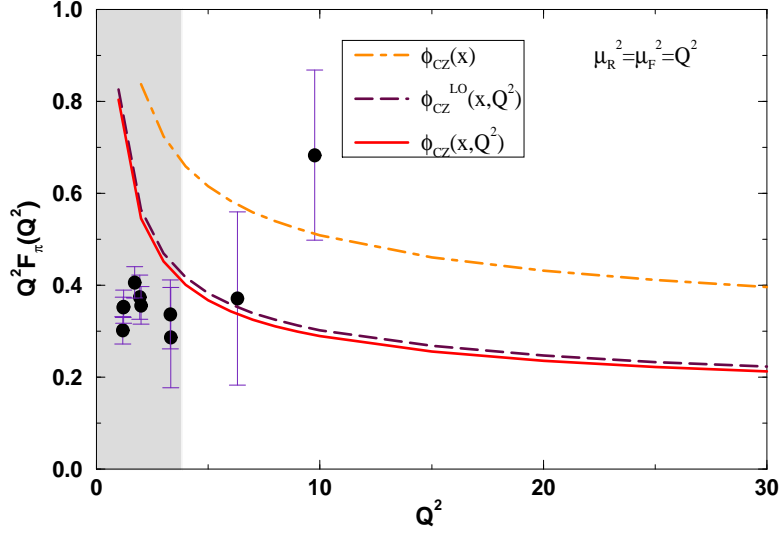


FIG. 9. Leading-twist NLO QCD predictions for the pion form factor, $Q^2 F_\pi(Q^2)$, obtained with the $\phi_{CZ}(x)$, $\phi_{CZ}^{LO}(x, \mu_F^2)$, and $\phi_{CZ}(x, Q^2)$ distributions.

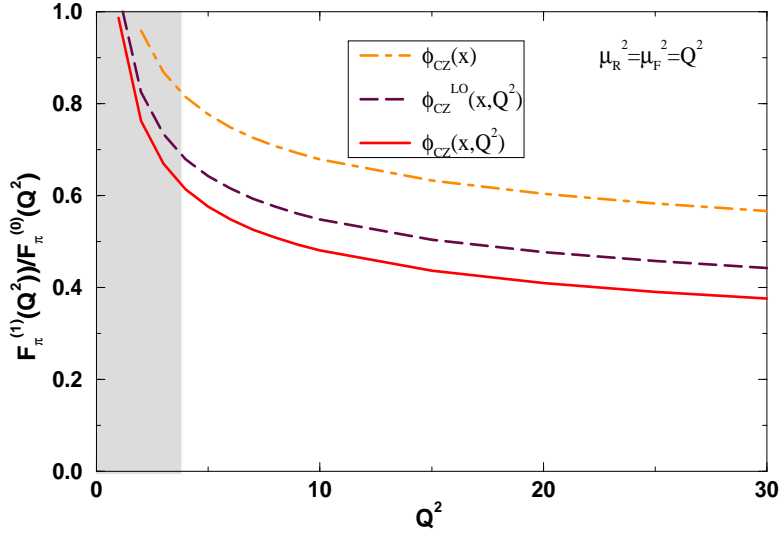


FIG. 10. The ratio of the NLO to the LO contributions to the pion form factor, $F_\pi^{(1)}(Q^2)/F_\pi^{(0)}(Q^2)$, obtained for the $\phi_{CZ}(x)$, $\phi_{CZ}^{LO}(x, \mu_F^2)$, and $\phi_{CZ}(x, Q^2)$ distributions. The shaded area denotes the region of Q^2 in which $\alpha_S(Q^2) > 0.3$.

TABLE VIII. The function $A_{UV}(\mu_R^2/Q^2)$ of Eq. (5.9) for different choices of μ_R^2 given by Eqs. (4.11, 4.21–4.23).

μ_R^2	$A_{UV}(\mu_R^2/Q^2)$	
	$\langle \bar{x} \rangle = 1/2$	$\langle \bar{x} \rangle = 1/3$
Q^2	2.62	
$\langle \bar{x} \rangle^2 Q^2$	1.63	1.04
$\langle \bar{x} \rangle^{3/2} Q^2$	1.88	1.44
$e^{-2/3} \langle \bar{x} \rangle^2 Q^2$	1.15	0.57

1. $\phi_{as}(x, \mu_F^2)$

A characteristic feature of the asymptotic distribution amplitude $\phi_{as}(x, \mu_F^2)$ is that it shows no evolution in the LO. In our notation, this means

$$\phi_{as}^{LO}(x, \mu_F^2) = \phi_{as}(x), \quad (5.6)$$

which, when taken into account in Eqs. (4.1–4.5), leads to the following expression for the form factor:

$$Q^2 F_\pi(Q^2, \mu_R^2, \mu_F^2) = (0.43 \text{ GeV}^2) \alpha_S(\mu_R^2) [1 + \alpha_S(\mu_R^2) A(\mu_R^2/Q^2, \mu_F^2/Q^2) + \alpha_S(\mu_F^2) B(\alpha_S(\mu_F^2))], \quad (5.7)$$

with the second and third terms inside the brackets arising from the NLO corrections to the hard-scattering amplitude and to the pion distribution amplitude, respectively.

The function $A(\mu_R^2/Q^2, \mu_F^2/Q^2)$, appearing in (5.7), is of the form

$$A(\mu_R^2/Q^2, \mu_F^2/Q^2) = A_{UV}(\mu_R^2/Q^2) + A_{IR}(\mu_F^2/Q^2) + A_C, \quad (5.8)$$

where the first term is

$$A_{UV}(\mu_R^2/Q^2) = \frac{4}{\pi} \int_0^1 dx \int_0^1 dy \frac{\phi_{as}(x) \phi_{as}(y)}{\bar{x} \bar{y}} f_{UV}(x, y, \mu_R^2/Q^2), \quad (5.9)$$

while the other two terms can be obtained from (5.9) by replacing the function f_{UV} by the functions f_{IR} and f_C , respectively. The functions f_{UV} , f_{IR} , and f_C are given by (2.12).

Now, owing to the fact that

$$\int_0^1 \int_0^1 dx dy \phi_{as}(y) \frac{(3 + \ln(\bar{x} \bar{y}))}{(\bar{x} \bar{y})} \phi_{as}(x) = 0,$$

one finds that the second term in (5.8) does not depend on μ_F^2 , and that its value is

$$A_{IR}(\mu_F^2/Q^2) = 0.27. \quad (5.10)$$

As for the third term in (5.8), one gets

$$A_C = -1.51. \quad (5.11)$$

Now, with the help of Eqs. (5.8), (5.10), and (5.11) it is possible to write

$$Q^2 F_\pi(Q^2, \mu_R^2, \mu_F^2) = (0.43 \text{ GeV}^2) \alpha_S(\mu_R^2) \{1 + \alpha_S(\mu_R^2) [A_{UV}(\mu_R^2/Q^2) - 1.24] + \alpha_S(\mu_F^2) B(\alpha_S(\mu_F^2))\}. \quad (5.12)$$

It should be noted that the dependence on the scales μ_R and μ_F has been separated in the above expression. Thus, the second term in the brackets, arising from the one-loop corrections to the hard-scattering amplitude, depends on the renormalization scale μ_R , while the third term originating from the evolutional correction of the asymptotic distribution amplitude, depends on the factorization scale μ_F .

As we have seen in the preceding subsection, the NLO contribution is dominated by the second term in (5.12), with the contribution of the third term being of the order of 2%. By neglecting the evolutional corrections of the distribution amplitude, the expression (5.12) becomes independent of μ_F , and the result for the form factor is determined by the function $A_{UV}(\mu_R^2/Q^2)$ defined by (5.9). Values of this function for the choices of μ_R^2 given by Eqs. (4.11, 4.21–4.23), and for the average momentum fraction $\langle \bar{x} \rangle_{as} = 1/2, 1/3$, are listed in Table VIII.

TABLE IX. Values of the pion form factor $Q^2 F_\pi(Q^2)$ at $Q^2 = 25 \text{ GeV}^2$, obtained with the $\phi_{as}(x, \mu_F^2)$ distribution amplitude. Choices for μ_R^2 are those of Eqs. (4.11) and (4.21–4.23) and $\mu_F^2 = Q^2$. For a given μ_R^2 , results are given for both $\langle \bar{x} \rangle_{as} = 1/2$ obtained using (4.25) and for $\langle \bar{x} \rangle_{as} = 1/3$ obtained using (4.27).

μ_R^2	μ_F^2	$Q^2 F_\pi^{(0)}(Q^2)$		$Q^2 F_\pi^{(1)}(Q^2)$		$F_\pi^{(1)}(Q^2)/F_\pi^{(0)}(Q^2)$		$Q^2 F_\pi(Q^2)$	
		$\langle \bar{x} \rangle = 1/2$	$\langle \bar{x} \rangle = 1/3$	$\langle \bar{x} \rangle = 1/2$	$\langle \bar{x} \rangle = 1/3$	$\langle \bar{x} \rangle = 1/2$	$\langle \bar{x} \rangle = 1/3$	$\langle \bar{x} \rangle = 1/2$	$\langle \bar{x} \rangle = 1/3$
Q^2	Q^2	0.094		0.026		0.277		0.120	
$\langle \bar{x} \rangle^2 Q^2$	Q^2	0.119	0.142	0.010	-0.012	0.085	-0.087	0.129	0.130
$\langle \bar{x} \rangle^{3/2} Q^2$	Q^2	0.112	0.126	0.016	0.005	0.142	0.036	0.127	0.130
$e^{-2/3} \langle \bar{x} \rangle^2 Q^2$	Q^2	0.137	0.169	-0.007	-0.048	-0.051	-0.285	0.130	0.121

TABLE X. Variation with Q^2 of the coupling constant $\alpha_S(\mu_R^2)$ of Eq. (2.2) for the choices of μ_R^2 given by Eqs. (4.11, 4.21–4.23), and $\langle \bar{x} \rangle = 1/2$ obtained using Eq. (4.25).

Q^2	$\alpha_S(\mu_R^2)$			
	μ_R^2			
	Q^2	$\langle \bar{x} \rangle^2 Q^2$	$\langle \bar{x} \rangle^{3/2} Q^2$	$e^{-2/3} \langle \bar{x} \rangle^2 Q^2$
4	0.303	0.434	0.392	0.547
5	0.289	0.406	0.369	0.503
10	0.253	0.338	0.312	0.403
15	0.236	0.308	0.286	0.360
20	0.225	0.289	0.270	0.336
25	0.217	0.276	0.259	0.318
30	0.211	0.267	0.250	0.306
40	0.202	0.253	0.238	0.288
50	0.196	0.243	0.229	0.275
100	0.178	0.217	0.206	0.242

Apart from being small, the term $\alpha_S(\mu_F^2)B(\alpha_S(\mu_F^2))$ in (5.12) depends on μ_F^2 very weakly. Thus, for fixed μ_R^2 and for the choices $\mu_F^2 = Q^2$ and $\mu_F^2 = \langle \bar{x} \rangle^2 Q^2$, with $\langle \bar{x} \rangle_{as} = 1/2, 1/3$, formula (5.12) leads to practically the same results. For this reason, when using the asymptotic distribution amplitude, we take $\mu_F^2 = Q^2$.

Our complete NLO results for the pion form factor obtained with the asymptotic distribution amplitude $\phi_{as}(x, \mu_F^2)$, with the choices for μ_R^2 given by Eqs. (4.21–4.23) and $\mu_F^2 = Q^2$, are summarized in Figs. 11, 12, 13, 14, and in Table IX. For the sake of the discussion of the validity of the predictions obtained, in Tables X and XI we give a variation (with Q^2) of the effective coupling $\alpha_S(\mu_R^2)$ of Eq. (2.2) for the choices of μ_R^2 given by Eqs. (4.11, 4.21–4.23). Tables X and XI assume $\langle \bar{x} \rangle_{as} = 1/2$ and $\langle \bar{x} \rangle_{as} = 1/3$, respectively. The results for the quantities $Q^2 F_\pi(Q^2)$ and $F_\pi^{(1)}(Q^2)/F_\pi^{(0)}(Q^2)$, obtained using $\langle \bar{x} \rangle_{as} = 1/2$, are plotted in Figs. 11 and 12, respectively. Predictions for the same quantities, but with $\langle \bar{x} \rangle_{as} = 1/3$, are shown in Figs. 13 and 14. Table IX provides a list of the relative contributions of various parts comprising the full NLO result for the pion form factor at the momentum transfer $Q^2 = 25 \text{ GeV}^2$, for the four choices of μ_R^2 and two values of $\langle \bar{x} \rangle_{as}$. The solid curves in Figs. 11–14 correspond to the results for $\mu_R^2 = \mu_F^2 = Q^2$ obtained in the preceding subsection.

Some comments are in order. By looking at Figs. 11–14, one notices that the scale choice $\mu_R^2 = \mu_F^2 = Q^2$, when compared with the other possibilities considered, leads, on the one hand, to the lowest values for $Q^2 F_\pi(Q^2)$ and, on the other hand, to the highest value for the ratio $F_\pi^{(1)}(Q^2)/F_\pi^{(0)}(Q^2)$. Next, as it is seen from Fig. 11, the prediction of $Q^2 F_\pi(Q^2)$ is essentially independent of the choice of μ_R^2 . Also, comparing Figs. 11 and 13 one sees that, for given μ_R^2 , the results do not change noticeably if one uses $\langle \bar{x} \rangle_{as} = 1/3$ instead of $\langle \bar{x} \rangle_{as} = 1/2$. By contrast, as Figs. 12 and 14 and Table IX show, the results for the ratio $F_\pi^{(1)}(Q^2)/F_\pi^{(0)}(Q^2)$ are sensitive to the choice of both μ_R^2 and $\langle \bar{x} \rangle_{as}$. For given μ_R^2 , the magnitude as well as (in some cases) the sign of the NLO correction are changed if the value $\langle \bar{x} \rangle_{as} = 1/3$ is used instead of $\langle \bar{x} \rangle_{as} = 1/2$.

We now comment on the reliability of the results displayed in Figs. 11–14. Imposing the requirements $F_\pi^{(1)}(Q^2)/F_\pi^{(0)}(Q^2) < 0.3$, and $\alpha_S(\mu_R^2) < 0.3$ and using the values of $\alpha_S(\mu_R^2)$ given in Tables X and XI, we find that the results corresponding to $\mu_R^2 = Q^2$, $\langle \bar{x} \rangle^2 Q^2$, $\langle \bar{x} \rangle^{3/2} Q^2$, and $e^{-2/3} \langle \bar{x} \rangle^2 Q^2$ are reliable for $Q^2 > 15, 15, 15$, and 30 GeV^2 , respectively, with $\langle \bar{x} \rangle_{as} = 1/2$, and for $Q^2 > 15, 40, 20$, and 60 GeV^2 , respectively, if $\langle \bar{x} \rangle_{as} = 1/3$ is used. We see that the “best” predictions are obtained with the choice $\mu_R^2 = \langle \bar{x} \rangle^{3/2} Q^2$.

Thus, if μ_R^2 is chosen to be of the order of average virtuality of the particles in the parton subprocess, reliable

TABLE XI. Same as Table X but with $\langle \bar{x} \rangle_{as} = 1/3$ obtained using Eq. (4.27).

Q^2	$\alpha_S(\mu_R^2)$			
	μ_R^2			
	Q^2	$\langle \bar{x} \rangle_{as}^2 Q^2$	$\langle \bar{x} \rangle_{as}^{3/2} Q^2$	$e^{-2/3} \langle \bar{x} \rangle_{as}^2 Q^2$
4	0.303	0.580	0.472	0.803
5	0.289	0.531	0.439	0.712
10	0.253	0.420	0.361	0.526
15	0.236	0.375	0.326	0.456
20	0.225	0.348	0.306	0.417
25	0.217	0.329	0.292	0.391
30	0.211	0.316	0.281	0.372
40	0.202	0.297	0.266	0.346
50	0.196	0.283	0.255	0.327
100	0.178	0.248	0.226	0.282

TABLE XII. Same as Table X but with $\langle \bar{x} \rangle_{CZ}(Q^2)$ obtained using Eq. (4.27).

Q^2	$\alpha_S(\mu_R^2)$			
	μ_R^2			
	Q^2	$\langle \bar{x} \rangle_{CZ}^2 Q^2$	$\langle \bar{x} \rangle_{CZ}^{3/2} Q^2$	$e^{-2/3} \langle \bar{x} \rangle_{CZ}^2 Q^2$
4	0.303	0.790	0.564	1.269
5	0.289	0.696	0.515	1.042
10	0.253	0.509	0.406	0.673
15	0.236	0.441	0.362	0.558
20	0.225	0.402	0.336	0.498
25	0.217	0.377	0.318	0.460
30	0.211	0.358	0.305	0.432
40	0.202	0.333	0.287	0.396
50	0.196	0.315	0.274	0.371
100	0.178	0.271	0.240	0.312

perturbative predictions for the pion form factor, based on the $\phi_{as}(x, \mu_F^2)$ distribution amplitude, can be obtained for momentum transfers $Q^2 > 15 \text{ GeV}^2$, with the NLO correction being of the order of 20%.

2. $\phi_{CZ}(x, \mu_F^2)$

Next, we present the NLO predictions for the form factor obtained with the $\phi_{CZ}(x, \mu_F^2)$ distribution amplitude, for various choices of μ_R^2 and μ_F^2 given by Eqs. (4.11, 4.21–4.23) and (4.15) and (4.24), respectively, and for the two ways, (4.25) and (4.27), for calculating the average momentum fraction $\langle \bar{x} \rangle_{CZ}(\mu_F^2)$.

Figures 15 and 16 show the results for $Q^2 F_\pi(Q^2)$ and $F_\pi^{(1)}(Q^2)/F_\pi^{(0)}(Q^2)$, respectively, using $\langle \bar{x} \rangle_{CZ} = 1/2$. The results for the same quantities but obtained for $\langle \bar{x} \rangle_{CZ}(\mu_F^2)$ are shown in Figs. 17 and 18. The solid curves in these figures are the results corresponding to $\mu_R^2 = \mu_F^2 = Q^2$, and are obtained in the preceding subsection. Various contributions to $Q^2 F_\pi(Q^2)$ at the momentum transfer $Q^2 = 25 \text{ GeV}^2$ are listed in Table XIII. For a given μ_F^2 , we have examined the sensitivity of the results to the values of μ_F^2 and found that, for the range of values $Q^2/2 < \mu_F^2 < Q^2$, the results are very stable. The values of $\alpha_S(\mu_F^2)$ needed when discussing the validity of the results obtained with $\langle \bar{x} \rangle_{CZ} = 1/2$ and $\langle \bar{x} \rangle_{CZ}(Q^2)$ are listed in Tables X and XII, respectively.

Some remarks are in order. First of all, it is interesting to note that the predictions based on the $\phi_{as}(x, \mu_F^2)$ and $\phi_{CZ}(x, \mu_F^2)$ amplitudes almost share the qualitative features, even though these two distributions are quite different in shape. Thus, as in the case of the $\phi_{as}(x, \mu_F^2)$ distribution amplitude, we see from Fig. 15 that the full NLO prediction is practically insensitive to the choice of the renormalization scale μ_R^2 . Comparison of Figs. 15 and 17 indicates that the results do not change noticeably if $\langle \bar{x} \rangle_{CZ}(Q^2)$ from Table III is used instead of $\langle \bar{x} \rangle_{CZ} = 1/2$. As far as the result for the ratio $F_\pi^{(1)}(Q^2)/F_\pi^{(0)}(Q^2)$ is concerned, Figs. 16 and 18 reveal that it is quite sensitive to the choices of both μ_R^2 and $\langle \bar{x} \rangle_{CZ}$.

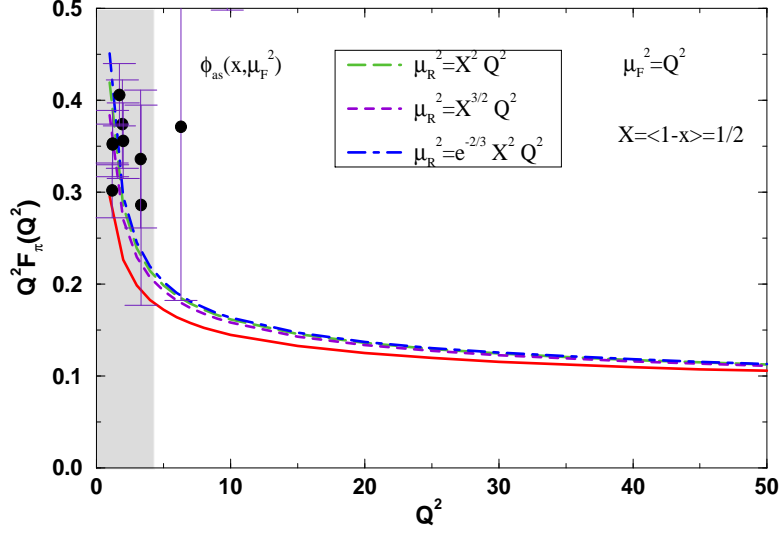


FIG. 11. Leading-twist NLO QCD results for $Q^2 F_\pi(Q^2)$ obtained with the $\phi_{as}(x, \mu_F^2)$ distribution amplitude and the choices of μ_R^2 given by Eqs. (4.21–4.23), with $\mu_F^2 = Q^2$ and $\langle \bar{x} \rangle_{as} = 1/2$. The solid curve (included for comparison) corresponds to the case $\mu_R^2 = \mu_F^2 = Q^2$ considered in the preceding subsection.

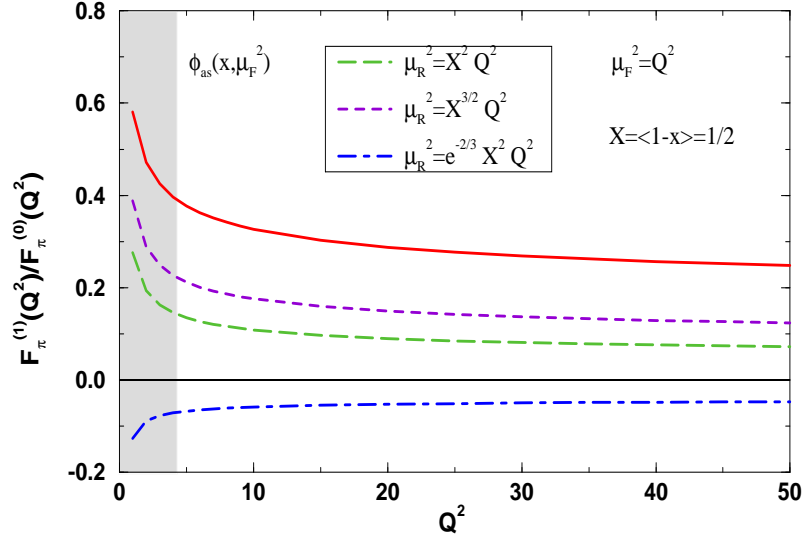


FIG. 12. The ratio $F_\pi^{(1)}(Q^2)/F_\pi^{(0)}(Q^2)$ obtained with the $\phi_{as}(x, \mu_F^2)$ distribution amplitude and the choices of μ_R^2 given by Eqs. (4.21–4.23), with $\mu_F^2 = Q^2$ and $\langle \bar{x} \rangle_{as} = 1/2$. The solid curve (included for comparison) is for the result corresponding to $\mu_R^2 = \mu_F^2 = Q^2$ obtained in the preceding subsection.

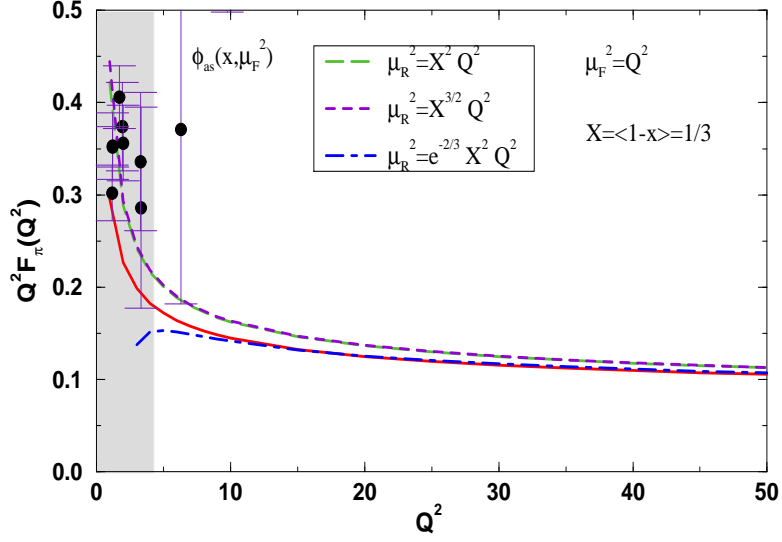


FIG. 13. Same as Fig. 11 but for $\langle \bar{x} \rangle_{as} = 1/3$.

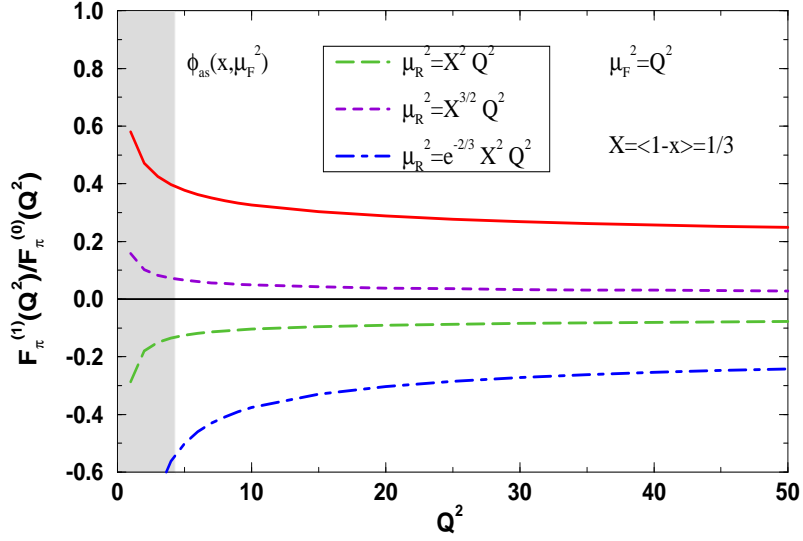


FIG. 14. Same as Fig. 12 but for $\langle \bar{x} \rangle_{as} = 1/3$.

TABLE XIII. Values of the pion form factor $Q^2 F_\pi(Q^2)$ at $Q^2 = 25 \text{ GeV}^2$, obtained with the $\phi_{CZ}(x, \mu_F^2)$ distribution amplitude. Choices for μ_R^2 are those of Eqs. (4.11) and (4.21–4.23) and $\mu_F^2 = Q^2$. For a given μ_R^2 , the results are given for both $\langle \bar{x} \rangle_{CZ} = 1/2$ obtained by (4.25), and $\langle \bar{x} \rangle_{CZ}(Q^2)$ obtained by (4.27), with the values listed in Table III.

μ_R^2	μ_F^2	$Q^2 F_\pi^{(0)}(Q^2)$		$Q^2 F_\pi^{(1)}(Q^2)$		$F_\pi^{(1)}(Q^2)/F_\pi^{(0)}(Q^2)$		$Q^2 F_\pi(Q^2)$	
		$\langle \bar{x} \rangle = 0.5$	$\langle \bar{x} \rangle_{CZ}(Q^2)$	$\langle \bar{x} \rangle = 0.5$	$\langle \bar{x} \rangle_{CZ}(Q^2)$	$\langle \bar{x} \rangle = 0.5$	$\langle \bar{x} \rangle_{CZ}(Q^2)$	$\langle \bar{x} \rangle = 0.5$	$\langle \bar{x} \rangle_{CZ}(Q^2)$
Q^2	Q^2	0.160		0.062		0.390		0.222	
Q^2	$\langle \bar{x} \rangle Q^2$	0.165		0.061		0.367		0.226	
$\langle \bar{x} \rangle^2 Q^2$	Q^2	0.204	0.278	0.049	-0.003	0.241	-0.010	0.253	0.275
$\langle \bar{x} \rangle^{3/2} Q^2$	Q^2	0.191	0.234	0.055	0.032	0.286	0.137	0.245	0.267
$e^{-2/3} \langle \bar{x} \rangle^2 Q^2$	Q^2	0.235	0.339	0.032	-0.074	0.136	-0.217	0.267	0.265
$\langle \bar{x} \rangle^2 Q^2$	$\langle \bar{x} \rangle Q^2$	0.211		0.045		0.211		0.255	
$\langle \bar{x} \rangle^{3/2} Q^2$	$\langle \bar{x} \rangle Q^2$	0.197		0.051		0.257		0.248	
$e^{-2/3} \langle \bar{x} \rangle^2 Q^2$	$\langle \bar{x} \rangle Q^2$	0.243		0.025		0.101		0.267	

Now, applying the same criteria for the reliability of our results as in the case of the $\phi_{as}(x, \mu_F^2)$ distribution amplitude and using Tables X and XII, we find that the results obtained with $\mu_R^2 = Q^2$, $\langle \bar{x} \rangle^2 Q^2$, $\langle \bar{x} \rangle^{3/2} Q^2$, and $e^{-2/3} \langle \bar{x} \rangle^2 Q^2$ are reliable for $Q^2 > 100, 15, 20$, and 30 GeV^2 , respectively, if $\langle \bar{x} \rangle_{CZ} = 1/2$, and for $Q^2 > 100, 60, 30$, and 100 GeV^2 if the values for $\langle \bar{x} \rangle_{CZ}(Q^2)$ given in Table III are used. Here, again, as in the case of the $\phi_{as}(x, \mu_F^2)$ distribution, the “best” result corresponds to the choice $\mu_R^2 = \langle \bar{x} \rangle^{3/2} Q^2$.

Therefore, choosing μ_R^2 to be of the same order as the average virtuality of the internal lines in the corresponding Feynman diagrams, reliable perturbative predictions for the pion form factor, using the $\phi_{CZ}(x, \mu_F^2)$ distribution amplitude, can be obtained for momentum transfers $Q^2 > 30 \text{ GeV}^2$, with the NLO correction being of order 20%.

C. Predictions obtained using the frozen coupling constant and $\mu_R^2 = a(x, y)Q^2$ and $\mu_F^2 = Q^2$

In the predictions obtained, we have assumed the form of the effective QCD coupling to be given by the usual one-loop formula (2.2), which, clearly, is not an accurate representation of the effective coupling at low momentum transfer. The actual behavior of the effective QCD coupling $\alpha_S(\mu_R^2)$ at low μ_R^2 , given by (2.2), is one of the key uncertainties in QCD phenomenology.

In this subsection instead of using Eq. (2.2), we use its modification given by the frozen coupling constant formula (4.28). With this form of the coupling, it is possible to use the choices for the scales μ_R^2 and μ_F^2 as they are given by Eqs. (4.12–4.14) and (4.16), respectively. For a given distribution amplitude and a specific choice of the scales μ_R^2 and μ_F^2 , the NLO expression for the form factor given by (4.1–4.5) can now be directly integrated.

Plotted in Figs. 19 and 20 are the NLO results for $Q^2 F_\pi(Q^2)$ and $F_\pi^{(1)}(Q^2)/F_\pi^{(0)}(Q^2)$, respectively, based on the $\phi_{as}(x, \mu_F^2)$ distribution amplitude and for different choices of the μ_R^2 of Eqs. (4.12–4.14) and $\mu_F^2 = Q^2$. The results for the same quantities but obtained using the $\phi_{CZ}(x, \mu_F^2)$ distribution are shown in Figs. 21 and 22. The results assume the frozen coupling constant formula (4.28) with the dynamical gluon mass $m_g^2 = 0.3 \text{ GeV}^2$ for which $\alpha_S(\mu_R^2) \leq \alpha_S(\mu_R^2 = 0 \text{ GeV}^2) = 0.41$. We have carried out an analysis of the sensitivity of our results to the value of m_g^2 and found that varying m_g^2 in the range $0.2 \leq m_g^2 \leq 0.3 \text{ GeV}^2$ only slightly influences the results. A comparison of the predictions for $Q^2 F_\pi(Q^2)$ obtained here, with the corresponding ones obtained in the previous subsections reveals that there are consistent with each other and that the former are somewhat less stable with respect to the variation of the renormalization scale μ_R than the latter. As a final observation, we note that the “best” prediction here is the one corresponding to the choice of μ_R given by Eq. (4.13).

VI. SUMMARY AND CONCLUSIONS

In this paper we have presented the results of a complete leading–twist NLO QCD analysis of the spacelike electromagnetic form factor of the pion at large momentum transfer.

To clarify the discrepancies in the analytical expression for the hard–scattering amplitude present in previous calculations, we have carefully recalculated the one–loop Feynman diagrams shown in Fig. 3. Working in the $\overline{\text{MS}}$

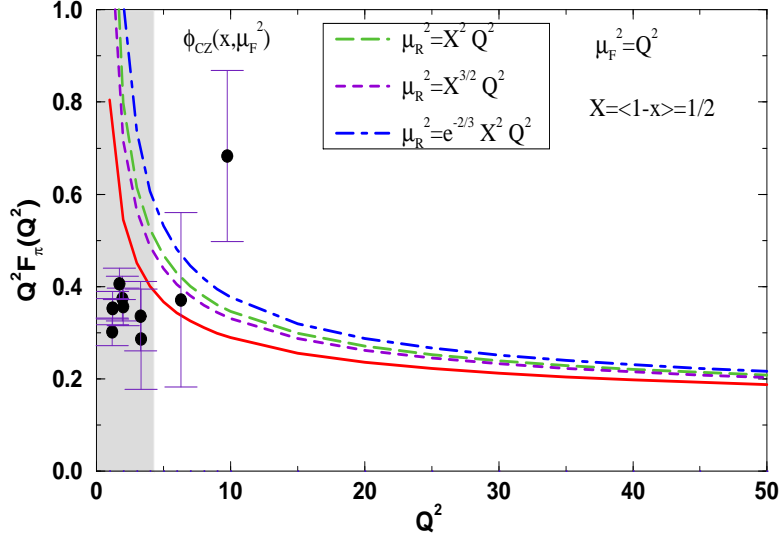


FIG. 15. Leading-twist NLO QCD results for $Q^2 F_\pi(Q^2)$ obtained with the $\phi_{CZ}(x, \mu_F^2)$ distribution amplitude and the choices of μ_R^2 given by Eqs. (4.21–4.23), with $\mu_F^2 = Q^2$ and $\langle \bar{x} \rangle_{CZ} = 1/2$. The solid curve (included for comparison) corresponds to the case $\mu_R^2 = \mu_F^2 = Q^2$ considered in the preceding subsection.

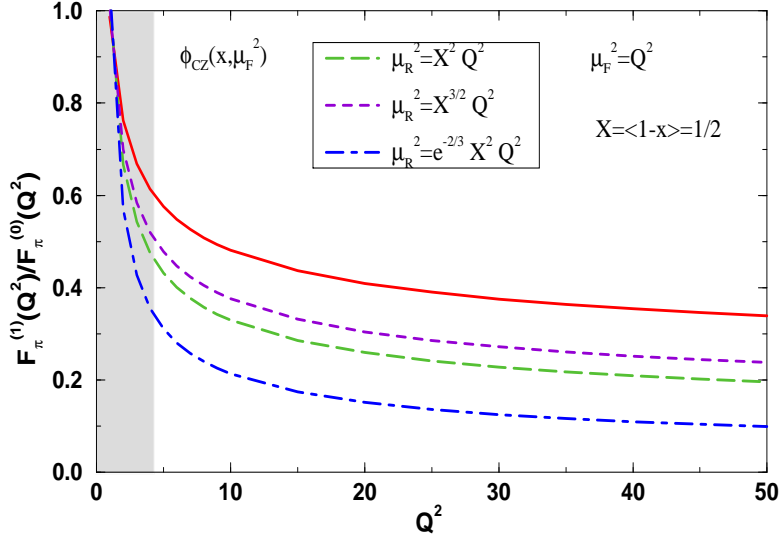


FIG. 16. The ratio $F_\pi^{(1)}(Q^2)/F_\pi^{(0)}(Q^2)$ obtained with the $\phi_{CZ}(x, \mu_F^2)$ distribution amplitude and the choices of μ_R^2 given by Eqs. (4.21–4.23), with $\mu_F^2 = Q^2$ and $\langle \bar{x} \rangle_{CZ} = 1/2$. The solid curve (included for comparison) is for the result corresponding to $\mu_R^2 = \mu_F^2 = Q^2$ obtained in the preceding subsection.

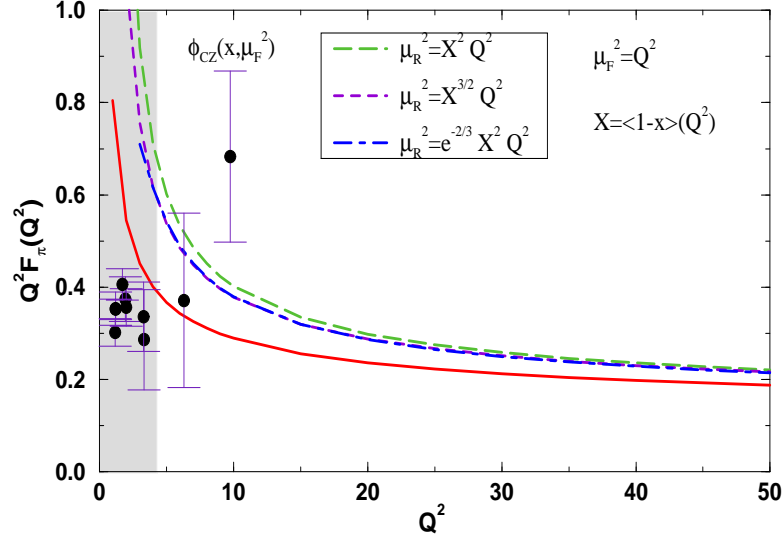


FIG. 17. Same as Fig. 15 but for $\langle \bar{x} \rangle_{CZ}(Q^2)$ given in Table III.

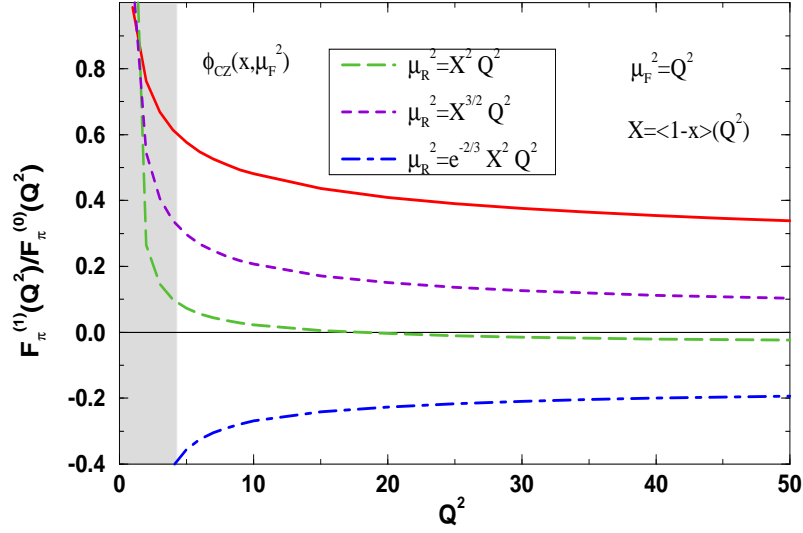


FIG. 18. Same as Fig. 16 but for $\langle \bar{x} \rangle_{CZ}(Q^2)$ given in Table III.

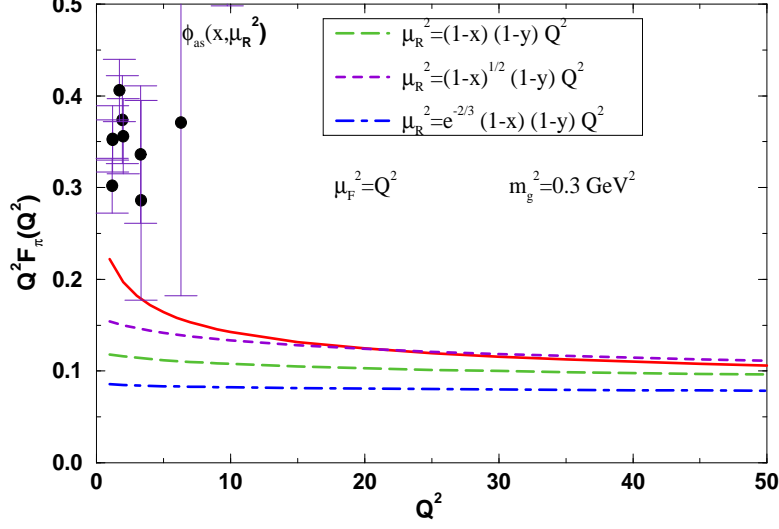


FIG. 19. Comparison with the existing experimental data of the leading-twist NLO QCD results for the pion form factor $Q^2 F_\pi(Q^2)$, based on the $\phi_{as}(x, \mu_F^2)$ distribution amplitude, for the choices of μ_R^2 of Eqs. (4.12–4.14) and $\mu_F^2 = Q^2$, and employing the frozen coupling constant formula (4.28) with $m_g^2 = 0.3 \text{ GeV}^2$. The solid curve (included for comparison) corresponds to the choice $\mu_R^2 = \mu_F^2 = Q^2$.

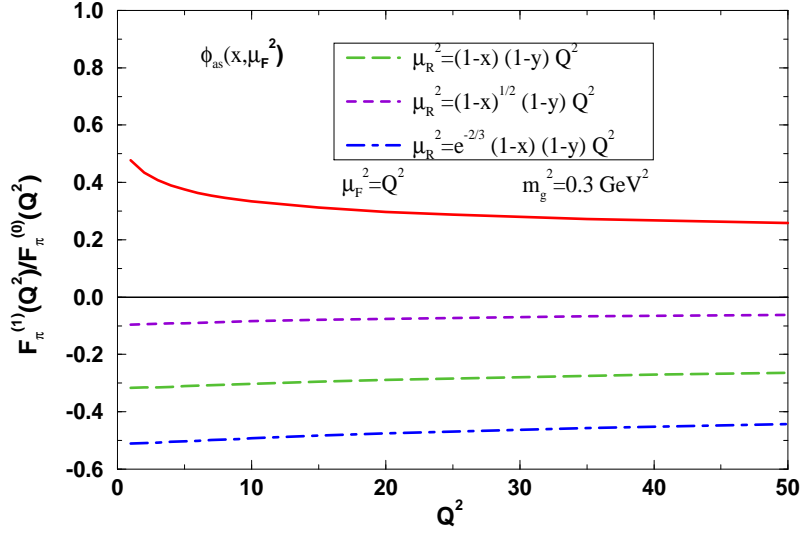


FIG. 20. The NLO prediction for the ratio $F_\pi^{(1)}(Q^2)/F_\pi^{(0)}(Q^2)$ based on the $\phi_{as}(x, \mu_F^2)$ distribution amplitude, for the choices of μ_R^2 of Eqs. (4.12–4.14) and $\mu_F^2 = Q^2$, and employing the frozen coupling constant formula (4.28) with $m_g^2 = 0.3 \text{ GeV}^2$. The solid curve (included for comparison) corresponds to the choice $\mu_R^2 = \mu_F^2 = Q^2$.

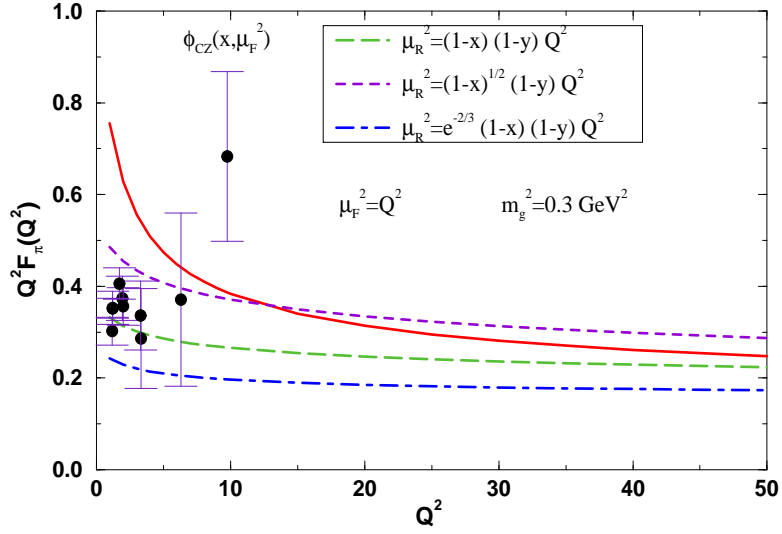


FIG. 21. The same as Fig. 19 but for $\phi_{CZ}(x, \mu_F^2)$ distribution amplitude.

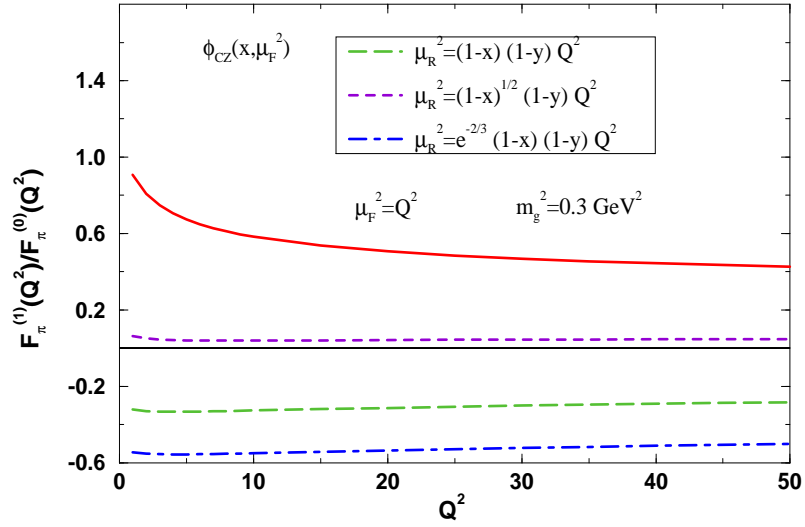


FIG. 22. The same as Fig. 20 but for $\phi_{CZ}(x, \mu_F^2)$ distribution amplitude.

scheme and employing the dimensional regularization method to treat all divergences (UV, IR, and collinear), we have obtained results which are in complete agreement with those of Ref. [9].

As nonperturbative input at the reference momentum scale of 0.5 GeV, we have used the four available pion distribution amplitudes defined by Eq. (3.16) and plotted in Fig. 4: the asymptotic distribution $\phi_{as}(x, \mu_F^2)$ and the three QCD sum-rule inspired distributions $\phi_{CZ}(x, \mu_F^2)$, $\phi_{P2}(x, \mu_F^2)$, and $\phi_{P3}(x, \mu_F^2)$. The NLO evolution of these distributions has been determined using the formalism developed in Ref. [20].

By convoluting according to Eq. (1.1), the hard-scattering amplitude with the pion distribution amplitude, both calculated in the NLO approximation, we have obtained the NLO numerical predictions for the pion form factor, for the four candidate distributions, and for several different choices of the renormalization and factorization scales, μ_R and μ_F . All the predictions have been obtained assuming $n_f = 3$ and $\Lambda_{\overline{MS}} = 0.2$ GeV.

To compare some of our predictions with those obtained previously, we have first used the choice of the scales where $\mu_R^2 = \mu_F^2 = Q^2$. The results are summarized in Figs. 7 and 8, and Tables IV–VII. Based on these results, we have been able to reduce the number of candidate distributions from four to two, namely, $\phi_{as}(x, \mu_F^2)$ and $\phi_{CZ}(x, \mu_F^2)$. The $\phi_{P2}(x, \mu_F^2)$ distribution leads to predictions practically identical to those obtained with $\phi_{CZ}(x, \mu_F^2)$, and as such need not be considered separately. As for the $\phi_{P3}(x, \mu_F^2)$ distribution, it can be discarded owing to a large deviation from the existing experimental data. Our results based on the asymptotic distribution amplitude $\phi_{as}(x, \mu_F^2)$ greatly differ from those of Ref. [5]. Thus, in contrast to Ref. [5], where it was concluded that “reliable perturbative predictions can not be made until momentum transfers, Q , of about 300–400 GeV are reached”, we have found that reliable predictions can already be made at momentum transfers of the order of 4–5 GeV. It has been shown that the inclusion of the NLO evolutional corrections only slightly influences the final result ($\sim 2\%$) if the $\phi_{as}(x, \mu_F^2)$ distribution is used, and leads to sizable effects (of order $\sim 7\%$) for the case of the $\phi_{CZ}(x, \mu_F^2)$ (and the other end-pointed distribution amplitudes).

In order to reduce the size of the NLO corrections and to examine the extent to which the NLO predictions for the pion form factor depend on the scales μ_R and μ_F , in addition to the simplest choice $\mu_R^2 = \mu_F^2 = Q^2$ (which certainly is not best suited for the process of interest), we have also considered the choices for μ_R and μ_F given by Eqs. (4.21–4.23) and (4.24), respectively. Using these alternative choices, and assuming the $\phi_{as}(x, \mu_F^2)$ and $\phi_{CZ}(x, \mu_F^2)$ pion distributions, leads to the predictions shown in Figs. 11–18. These predictions are remarkable in the sense that, for a given distribution amplitude, values of the pion form factor, $Q^2 F_\pi(Q^2)$, are almost insensitive to various choices of the scales μ_R and μ_F . This is evident from Figs. 11, 13, 15, and 17, and is a reflection of the stabilizing effect that the inclusion of the NLO corrections has on the LO predictions. On the other hand, the ratio of the NLO corrections to the LO prediction is very sensitive to the values of μ_R and μ_F . Requiring this ratio to be less than 0.3 and $\alpha_S(\mu_R^2) < 0.3$ (a rather stringent condition), we have found that the predictions obtained with the $\phi_{as}(x, \mu_F^2)$ and $\phi_{CZ}(x, \mu_F^2)$ distribution amplitudes can be considered reliable for the momentum transfers $Q^2 > 15$ GeV² and $Q^2 > 30$ GeV², respectively, with the NLO corrections to the LO results being, for both distributions of order 20%. The difference between the predictions based on these two distributions is large enough to allow an unambiguous experimental discrimination between the two possibilities as soon as the data extending to higher values of Q^2 become available. It is worth noting that the best predictions are obtained with μ_R^2 taken to be equal to the geometrical mean of the average gluon and quark virtualities in the process.

We have also examined to what extent our predictions for both distributions ($\phi_{as}(x, \mu_F^2)$, $\phi_{CZ}(x, \mu_F^2)$) depend on the form of the effective QCD coupling constant. We have found that the overall magnitude of $Q^2 F_\pi(Q^2)$ calculated with $\alpha_S(\mu_R^2)$ inside the integrals (4.1–4.5) and using the frozen coupling formula (4.28) agrees well with that calculated with $\alpha_S(\langle \mu_R^2 \rangle)$ based on the one-loop formula (2.2).

In conclusion, the results of the complete leading-twist NLO QCD analysis, which has been carried out in this paper, show that the reliable perturbative predictions for the pion form factor using the $\phi_{as}(x, \mu_F^2)$ and $\phi_{CZ}(x, \mu_F^2)$ distributions can already be made at the momentum transfer Q of about 4–5 GeV. To check our predictions and to choose between the two distributions it is necessary that the better experimental data are obtained.

ACKNOWLEDGMENTS

This work was supported by the Ministry of Science and Technology of the Republic of Croatia under the contract Nr. 00980102.

- [1] S. J. Brodsky and G. P. Lepage, Phys. Lett. **87B**, 359 (1979); Phys. Rev. Lett. **43**, 545 (1979); Phys. Rev. Lett. **43** (1979) 1625 (E); G. P. Lepage and S. J. Brodsky, Phys. Rev. D **22**, 2157 (1980).
- [2] A. V. Efremov and A. V. Radyushkin, Theor. Mat. Phys. **42**, 97 (1980); Phys. Lett. **94B**, 245 (1980).
- [3] A. Duncan and A. H. Mueller, Phys. Lett. **90B**, 159 (1980); Phys. Rev. D **21**, 1636 (1980).
- [4] S. J. Brodsky and G. P. Lepage, in *Perturbative QCD*, edited by A. H. Mueller (World Scientific Publishing Co., Singapore, 1989); V. L. Chernyak, in *High p_T Physics and Higher Twists*, Proceedings of the Conference, Paris, France, 1988, edited by M. Benayoun, M. Fontannaz, and J. L. Narjoux, [Nucl. Phys. Proc. Suppl. **7B**, 297 (1989)].
- [5] R. D. Field, R. Gupta, S. Otto, and L. Chang, Nucl. Phys. **B186**, 429 (1981).
- [6] F.-M. Dittes and A. V. Radyushkin, Yad. Fiz. **34**, 529 (1981), [Sov. J. Nucl. Phys. **34**, 293 (1981)].
- [7] M. H. Sarmadi, Ph. D. thesis, University of Pittsburgh, 1982.
- [8] A. V. Radyushkin and R. S. Khalmuradov, Yad. Fiz. **42**, 458 (1985), [Sov. J. Nucl. Phys. **42**, 289 (1985)].
- [9] E. Braaten and S.-M. Tse, Phys. Rev. D **35**, 2255 (1987).
- [10] E. P. Kadantseva, S. V. Mikhailov, and A. V. Radyushkin, Yad. Fiz. **44**, 507 (1986), [Sov. J. Nucl. Phys. **44**, 326 (1986)].
- [11] F. D. Aguila and M. K. Chase, Nucl. Phys. **B193**, 517 (1981).
- [12] E. Braaten, Phys. Rev. D **28**, 524 (1983).
- [13] B. Nizic, Phys. Rev. D **35**, 80 (1987).
- [14] N. Isgur and C. H. Llewellyn Smith, Phys. Rev. Lett. **52**, 1080 (1984); Phys. Lett. **217B**, 535 (1989); Nucl. Phys. **B 317**, 526 (1989).
- [15] A. V. Radyushkin, Nucl. Phys. **A 532**, 141 (1991).
- [16] H.-N. Li and G. Sterman, Nucl. Phys. **B 381**, 129 (1992); D. Tung and H.-N. Li, preprint CCUTH-97-06, hep-ph/9712541.
- [17] R. Jakob and P. Kroll, Phys. Lett. **315B**, 463 (1993); *ibid.* **319B**, 545 (E) (1993).
- [18] F.-M. Dittes and A. V. Radyushkin, Phys. Lett. **134B**, 359 (1984); M. H. Sarmadi, *ibid.* **143B**, 471 (1984); G. R. Katz, Phys. Rev. D **31**, 652 (1985); S. V. Mikhailov and A. V. Radyushkin, Nucl. Phys. **B254**, 89 (1985).
- [19] S. V. Mikhailov and A. V. Radyushkin, Nucl. Phys. **B273**, 297 (1986).
- [20] D. Müller, Phys. Rev. D **49**, 2525 (1994); Phys. Rev. D **51**, 3855 (1995).
- [21] V. L. Chernyak and A. R. Zhitnitsky, Phys. Rep. **112**, 173 (1984).
- [22] G. Martinelli and C. Sacharadja, Phys. Lett. **190B**, 151 (1987); Phys. Lett. **217B**, 319 (1989).
- [23] E. G. Floratos, D. A. Ross, and C. T. Sachrajda, Nucl. Phys. **B129**, 66 (1977); *ibid.* **B 139**, 545 (E) (1978).
- [24] A. Gonzales-Arroyo, C. Lopez, and F. J. Yndurain, Nucl. Phys. **B153**, 161 (1979).
- [25] G. R. Farrar, K. Huleihel, and H. Zhang, Nucl. Phys. **B349**, 655 (1991).
- [26] S. J. Brodsky, G. P. Lepage, and P. B. Mackenzie, Phys. Rev. D **28**, 228 (1983).
- [27] G. Parisi and R. Petronzio, Phys. Lett. **94B**, 51 (1980); A. C. Mattingly and P. M. Stevenson, Phys. Rev. D **49**, 437 (1994); V. N. Gribov, Lund Report No. LU-TP 91-7, 1991 (unpublished); K. D. Born, E. Laermann, R. Sommer, P. M. Zerwas, and T. F. Walsh, Phys. Lett. **329B**, 325 (1994); J. M. Cornwall, Phys. Rev. D **26**, 1453 (1982); A. Donnachie and P. V. Landshoff, Nucl. Phys. **B311**, 509 (1989).
- [28] M. B. Gay Ducati, F. Halzen, and A. A. Natale, Phys. Rev. D **48**, 2324 (1993).
- [29] J. Bebek et al., Phys. Rev. D **17**, 1693 (1978).
- [30] S. R. Amendolia et al., Nucl. Phys. **B277**, 168 (1986).
- [31] C. E. Carlson and J. Milana, Phys. Rev. Lett. **65**, 1717 (1990).
- [32] S. Dubnička and L. Martinovič, Phys. Rev. D **39**, 2079 (1989); J. Phys. G **15**, 1349 (1989).
- [33] A. V. Radyushkin, Acta Phys. Polon. **B26**, 2067 (1995); S. Ong, Phys. Rev. D **52**, 3111 (1995); P. Kroll and M. Raulfs, Phys. Lett. **387B**, 848 (1996).